2

BNL-47317
Informal Report

POLARIZED WIGGLER FOR NSLS X-RAY RING DESIGN CONSIDERATION

A. Friedman, S. Krinsky, E. Blum

March 1992

NATIONAL SYNCHROTRON LIGHT SOURCE

BROOKHAVEN NATIONAL LABORATORY
ASSOCIATED UNIVERSITIES, INC.

Under Contract No DE-AC02-76CH00016 with the
UNITED STATES DEPARTMENT OF ENERGY

BNL-47317
Informal Report

Polarized Wiggler for NSLS X-Ray Ring Design Considerations

BNL--47317

DE92 012212

A. Friedman, S. Krinsky, E. Blum

National Synchrotron Light Source

Brookhaven National Laboratory

Upton, New York 11973

March 1992

Polarized Wiggler for NSLS X-ray Ring Design Consideration*

A. Friedman, S. Krinsky and E. Blum

National Synchrotron Light Source
Brookhaven National Laboratory
Upton, NY 11973

Abstract

We examine the properties of an elliptically polarized wiggler that will generate circularly polarized photons with energy spectrum of 3–12 KeV. The vertical wiggler magnetic field is produced by permanent magnets while the horizontal wiggler field is generated by electric coils capable of AC excitation. The radiation parameters of the wiggler are presented, including photon flux, circular and linear polarization and spectrum. These parameters are compared to the synchrotron radiation from a bending magnet. Numerical values are calculated for radiation from the wiggler and bending magnet for the NSLS X-ray ring parameters. A conceptual design for such a wiggler is discussed and several different alternatives are analyzed. We consider AC excitation of the wiggler to produce the time modulation of the elliptic polarization, and also to produce time modulated linearly polarized radiation.

* Work performed under the auspices of the US Department of Energy under contract no. DE-AC02-76CH00016.

1. Introduction

Circularly polarized X-ray light is an essential tool in several research areas. Its main virtue is that magnetic properties can be detected much more easily with circularly polarized photons than with linearly polarized or unpolarized photons. Some effects can only be detected with circularly polarized photons. A typical experiment using circularly polarized light involves measuring the absorption or scattering of the photons by a target. Measurements are taken for right and left circular polarization. The results are then subtracted from each other in order to yield the net polarization. Fig. 1 illustrates a magnetic Compton scattering experiment involving a soft magnetic material[1]. An axial magnetic field is applied to the target and the scattered photon intensity I^+ is measured, the magnetic field is then reversed and the scattered photon intensity I^- is measured at the same angle. Since the material is soft, reversal of the magnetic field causes the spins to invert. Thus, $n_\uparrow$ becomes $n_\downarrow$ and $n_\downarrow$ becomes $n_\uparrow$ ($n_\uparrow$ being the number of electrons in spin up state, and $n_\downarrow$ the number of electrons in spin down state). The measured quantities I^+ and I^- can be calculated by:

$$\begin{aligned} I^+ &= (f^+ + f^-)(n_\uparrow + n_\downarrow)\Phi_0 + (f^+ - f^-)(n_\uparrow - n_\downarrow)\Phi_{spin} \\ I^- &= (f^+ + f^-)(n_\uparrow + n_\downarrow)\Phi_0 - (f^+ - f^-)(n_\uparrow - n_\downarrow)\Phi_{spin} \end{aligned} \tag{1}$$

where f^+, f^- are the fluxes of the right polarized and the left polarized incoming photons respectively, Φ_0 is the spin independent scattering cross section, and Φ_{spin} is the spin dependent component of the scattering cross section. The net spin of the material can be calculated from Eqs. 1:

$$\frac{I^+ - I^-}{I^+ + I^-} = \frac{f^+ - f^-}{f^+ + f^-}\frac{n_\uparrow - n_\downarrow}{n_\uparrow + n_\downarrow}\frac{\Phi_{spin}}{\Phi_0}. \tag{2}$$

In Eq. 2, $f^+ + f^-$ is the total photon flux and is measured separately, $n_\uparrow + n_\downarrow$ is usually known (for an element it is simply the atomic weight). Φ_0 and Φ_{spin} are calculated theoretically. Thus, either the net spin $n_\uparrow - n_\downarrow$ or the net circular polarization $f^+ - f^-$ can be determined from Eq. 2. This experimental setup can be used to measure the polarization of the incoming photons[1] ($P_c \equiv (f^+ - f^-)/(f^+ + f^-)$) by using a material in

which $(n_\uparrow - n_\downarrow)/(n_\uparrow + n_\downarrow)$ is known, such as soft iron. For a photon beam with a known P_c the experiment can be used to determine the net spin of a material. Note, that for a linearly polarized photon beam $f^+ - f^- = 0$, and hence Eq. 2 will not yield the net spin.

Hard ferromagnetic materials do not yield the same net spin when the DC magnetic field is reversed. It is, thus, beneficial to be able to reverse, instead, the helicity of the photon beam. Such reversal is also described by the relations of Eq. 2.

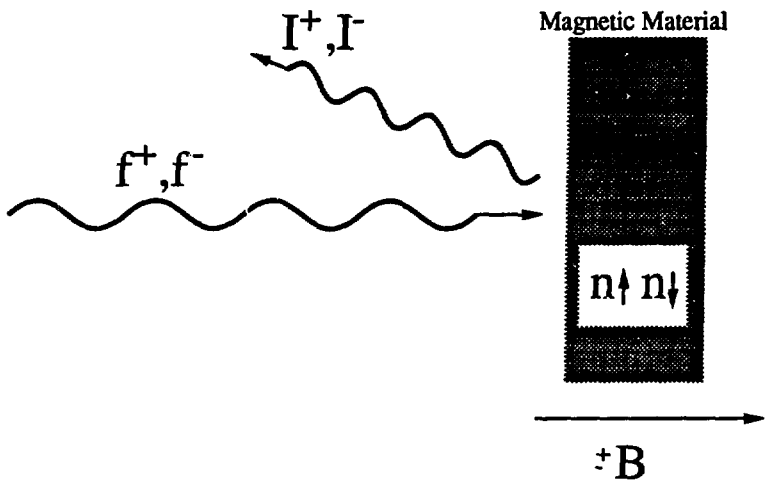

Figure 1: Magnetic Compton scattering experiment setup

In most cases[2] $\Phi_{spin}/\Phi_0 \ll 1$. Hence, the experiment described in Fig. 1 poses a serious detection problem. This problem may be alleviated by using an incoming photon beam in which the polarization is modulated in time.

$$P_c \approx P_{c_{max}} \cos \omega t. \tag{3}$$

As it will be demonstrated later the circular polarization dependence on the wiggler strength is not linear. Hence, for a sinusoidal magnetic field, P_c is not precisely sinusoidal, but has higher harmonic content. The signal detected with the P_c of Eq. 3 is

$$\frac{I^+ - I^-}{I^+ + I^-} \approx \frac{n_\uparrow - n_\downarrow}{n_\uparrow + n_\downarrow} \frac{\Phi_{spin}}{\Phi_0} P_{c_{max}} \cos \omega t, \tag{4}$$

where in this case I^+, I^- are the measurements for positive and negative helicity respectively. The measurement of the intensities $I^\pm$ is a small AC signal (spin effect) modulating

a large DC offset (charge effect). This AC signal can be readily detected using such techniques as lock-in amplifiers and high-pass filters. Fig. 2 describes an elliptically polarized wiggler[6,7] constructed from a vertical permanent magnet wiggler and a horizontal wiggler which may be constructed either of a permanent magnet[6,7] or an electromagnetic magnet[11]. In the case of an electromagnetic wiggler, the oscillation of P_c is achieved by exciting the wiggler with AC current. In this design, the horizontal and vertical wigglers are displaced relative to one another by 90°.

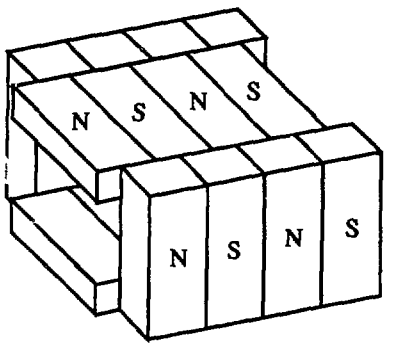

Figure 2: Schematic of an elliptically polarized wiggler

2. Electromagnetic Excitation and Polarization

2.1. Electromagnetic Excitation by a Charged Particle Beam

The electromagnetic field radiated by electrons passing through a wiggler can be calculated using standard techniques[5,12–14]. Here we apply an approach developed by Gover and Friedman[3]. The three dimensional Fourier decomposition of the electric field is given by[3]:

$$\mathbf{E}(\mathbf{r},t) = \sum_{\sigma} \frac{1}{(2\pi)^3} \int_{-\infty}^{\infty} d\omega dk_x dk_y \; \mathbf{e}_\sigma \chi(\omega,\mathbf{k}) e^{-i\omega t + i\mathbf{k}\cdot\mathbf{r}}, \tag{5}$$

where

$$k_z = \sqrt{\left(\frac{\omega}{c}\right)^2 - k_x^2 - k_y^2}, \tag{6}$$

$\mathbf{e}_\sigma$ is a unit vector denoting the field polarization, and the summation is over all the or-

thogonal polarizations σ. For a current of particles with charge $-e$, the Fourier component $\chi(\omega, \mathbf{k})$ is expressed in terms of the path integrals of the electromagnetic field along the particle trajectories:

$$\chi(\omega, \mathbf{k}) = e\frac{Z_0}{2}\sum_j \Delta W_j(\omega, \mathbf{k}), \tag{7}$$

where $Z_0 = \sqrt{\mu_0/\epsilon_0}$ is the vacuum impedance, the summation is over the charged particles and the path integral is:

$$\Delta W_j = \int_{-\infty}^{\infty} dt\ \mathbf{v}_j(t)\cdot\mathbf{e}_\sigma e^{-i\mathbf{k}\cdot\mathbf{r}_j(t)+i\omega t}. \tag{8}$$

In Eq. 8, $\mathbf{v}_j(t)$, $\mathbf{r}_j(t)$ are the velocity and trajectory of the j-th particle. The photon flux per solid angle can be calculated[8] from Eqs. 5–8

$$\frac{dN}{dtd\Omega} = \frac{1}{(2\pi)^2}\alpha\frac{1}{c^2}\frac{I}{e}\omega^2\left(\frac{\Delta\omega}{\omega}\right)\left\langle|\Delta W_j|^2\right\rangle_j, \tag{9}$$

where $\alpha = e^2/2\epsilon_0 hc = 1/137.04$ is the fine structure constant, I is the beam current and $\Delta\omega/\omega$ is the measured bandwidth. For high energy photons it is convenient to express the flux in terms of photon energy instead of photon frequency:

$$\frac{dN}{dtd\Omega} = \alpha\frac{e}{(hc)^2} I\, V_{ph}^2\left(\frac{\Delta\omega}{\omega}\right)\left\langle|\Delta W_j|^2\right\rangle_j, \tag{10}$$

where V_{ph} is the photon energy in electron volts.

2.2. Photon Polarization

From Eq. 8 it can be seen that there is a direct relation between the electron velocity vector and the polarization. In fact, Eq. 8 suggests that the polarization of the radiated photon is the projection of the electron velocity vector on the plane normal to the line connecting the viewer to the source (Fig. 3a). It is, thus, easy to see that a particle moving on a circular trajectory will generate elliptically polarized radiation, depending on the viewing angle (Fig. 3b). In reality, the dependence of the polarization on the particle parameters is more complex. Eq. 8 involves an integration over time, and different components of the velocity may have different time behavior, resulting in a complicated

function for the polarization. As discussed in the next section, a high degree of circular polarization of synchrotron radiation is achieved at small angles for photon energies near the critical energy*.

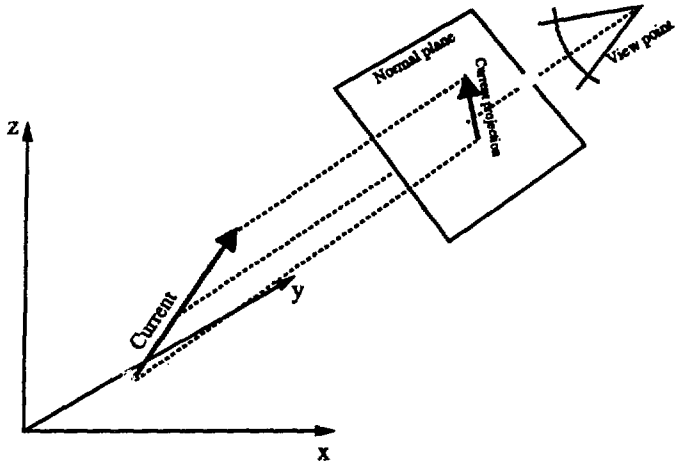

(a)

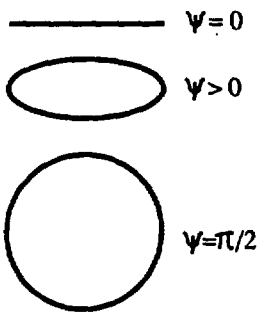

(b)

Figure 3: Polarization as a function of view angle (a) linear polarization (b) circular polarization.

In many cases, the electron beam emittance is large enough to affect the polarization. Hence, statistical methods should be used to analyze the degree of polarization produced. We define the coherence matrix[4,17,18]:

* The critical energy $\hbar\omega_c$ is the energy above which the photon flux drops rapidly.

$$J \equiv \begin{pmatrix} \langle E_x E_x^* \rangle & \langle E_x E_y^* \rangle \\ \langle E_y E_x^* \rangle & \langle E_y E_y^* \rangle \end{pmatrix} \equiv \begin{pmatrix} J_{xx} & J_{xy} \\ J_{yx} & J_{yy} \end{pmatrix}. \tag{11}$$

In Eq. 11; x,y stand for the directions in the plane perpendicular to the viewer, and the symbol <> stands for averaging over the different emitters (electrons). For unpolarized light

$$J_{xx} = J_{yy} \; ; \quad J_{xy} = J_{yx} = 0. \tag{12}$$

The polarization can be defined by the four dimensional Stokes vector[17]:

$$\begin{aligned} &S_0 \equiv J_{xx} + J_{yy} \; ; \; \text{Total intensity.} \\ &S_1 \equiv J_{xx} - J_{yy} \; ; \; \text{Polarization in the x or y direction.} \\ &S_2 \equiv J_{xy} + J_{yx} \; ; \; \text{Polarization in the 45° or 135° direction.} \\ &S_3 \equiv -i(J_{xy} - J_{yx}) \; ; \; \text{Circular polarization.} \end{aligned} \tag{13}$$

The degree of polarization is

$$P \equiv \frac{\sqrt{S_1^2 + S_2^2 + S_3^2}}{S_0} \leq 1, \tag{14}$$

the degree of circular polarization is

$$P_c = \frac{S_3}{S_0}, \tag{15}$$

and the degree of linear polarization is

$$P_L = \frac{\sqrt{S_1^2 + S_2^2}}{S_0}. \tag{16}$$

Note that $P_c = P$ implies $P_L = 0$ and vice versa. Thus, elliptically polarized light may be regarded as consisting of circular polarization plus linear polarization.

3. Synchrotron Radiation

Consider an electron rotating in a circular trajectory with radius ρ and linear velocity $v = \beta c$ in the xz plane (Fig. 4).

$$x = \rho \cos \frac{\beta ct}{\rho} \; ; \quad z = \rho \sin \frac{\beta ct}{\rho}. \tag{17}$$

Since the trajectory is a perfect circle, the radiation does not depend on the horizontal angle ξ, but only on the vertical angle ψ ($\psi \equiv \pi/2 - \theta$). For radiation frequencies much larger than the rotation frequency, most of the radiation comes from a small arc near the tangential point between viewing line and the circle. Hence, the t dependence in Eq. 8 can be expanded in a Taylor series around $t(\xi = 0)$. Performing this expansion to third order and carrying out the integration results in[5]:

$$\begin{aligned} \Delta W_\theta &= \frac{2}{\sqrt{3}} \rho \psi \sqrt{\frac{1}{\gamma^2} + \psi^2}\, K_{1/3}(\eta) \\ \Delta W_\xi &= -i \frac{2}{\sqrt{3}} \rho \left(\frac{1}{\gamma^2} + \psi^2 \right) K_{2/3}(\eta) \\ \eta &= \frac{\omega}{2\omega_c} \left(1 + \gamma^2 \psi^2\right)^{3/2} \\ \omega_c &= \frac{3}{2} \frac{\gamma^3 c}{\rho} \end{aligned} \tag{18}$$

where γ is the Lorentz factor and $K_{1/3}$, $K_{2/3}$ are modified Bessel functions. From Eq. 18 it is obvious that the radiation in the plane of the circular orbit is perfectly linearly polarized and as the vertical angle ψ grows, the radiation becomes more and more circularly polarized.

By Eq. 10, the photon flux ($photons/sec/rad^2$) is:

$$\frac{dN}{dt\, d\Omega} = \frac{4}{3} \alpha \frac{e}{(hc)^2} I V_{ph}^2 \rho^2 \left(\frac{\Delta\omega}{\omega} \right) \left(\frac{1}{\gamma^2} + \psi^2 \right) \left[\psi^2 K_{1/3}^2(\eta) + \left(\frac{1}{\gamma^2} + \psi^2 \right) K_{2/3}^2(\eta) \right]. \tag{19}$$

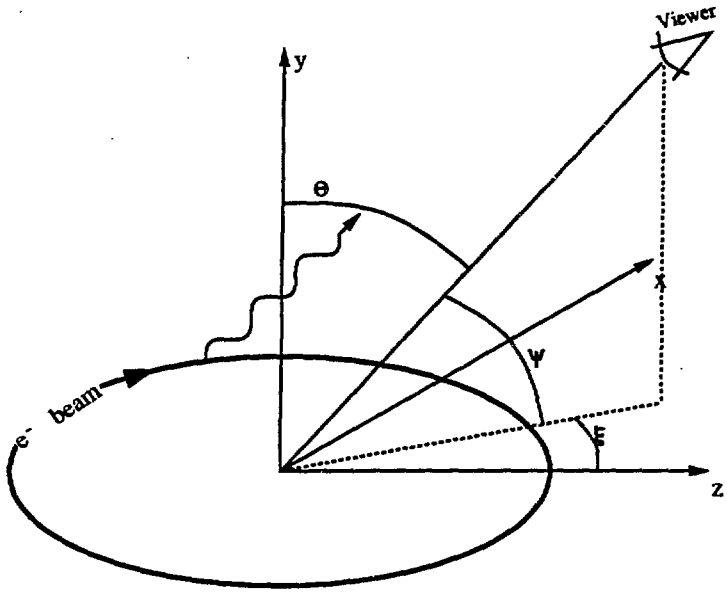

Figure 4: Storage ring trajectory

Figs. 5 and 6 show the photon flux and polarization that can be achieved from the bending magnets of the NSLS X-ray storage ring. In these figures, we take a conservative estimate of the vertical emittance of the X-ray ring ($\epsilon_y = 2 \times 10^{-9}$m rad) and consider the beta function at the source to be ($\beta_y = 16$m, $\sigma_{y'} = 11\mu$rad). Calculations were carried out by averaging over the electron vertical angle distribution. Fig. 5a shows the circular and linear polarizations as a function of photon energy, measured at $\psi = 1/2\gamma$. Note, that for very high photon energies ($\omega \gg \omega_c$) the circular polarization decreases and the linear polarization increases. This happens beacause the circular polarization becomes more sensitive to the electron beam angular spread for increasing photon energy while the linear polarization becomes less sensitive. For a filament beam (zero emittance) the linear and circular polarizations approach an asymptotic limit as the photon energy increases above the critical energy:

$$P_{L\infty} = \frac{1}{1+2\psi_n^2}$$
$$P_{C\infty} = \frac{2\psi_n\sqrt{1+\psi_n^2}}{1+2\psi_n^2} \qquad (20)$$

where

$$\psi_n \equiv \gamma\psi \tag{21}$$

is the normalized angle. For $\psi_n = 1/2$, $P_{L\infty} = 2/3$ and $P_{c\infty} = \sqrt{5}/3$.

Fig. 6a shows the angular dependence of the polarization for a photon energy of 10KeV. The circular polarization grows and the linear polarization decreases with the angle. Although not shown in the figures, the total polarization is constant in photon energy and angle and is a function of the angular spread only. Figs. 5b and 6b show the photon flux as a function of photon energy and vertical angle respectively.

From Figs. 5 and 6 it is obvious that circularly polarized light is produced in a storage ring bending magnet. Unfortunately, since it is only detected off the ring plane, the flux is low and for many experiments insufficient. Another disadvantage of using a bending magnet as a source of circularly polarized radiation is that the synchrotron radiation from a bending magnet does not vary with time. Although a time varying orbit could, in principle, be used to change the angle between the irradiated object and the electron beam, thereby varying the degree of circular polarization, such techniques are complicated and could endanger the orbit stability of the whole storage ring. Thus, in order to use AC techniques for signal detection, it is of significant interest to build an insertion device that will generate a high flux of circularly polarized light with AC modulation of the polarization.

Fig. 7 shows how the polarization and the photon flux vary as a function of the vertical angular spread of the electron beam. The circular polarization decreases drastically for increasing angular spread, while the linear polarization increases. This results from the cancellation of the component of the electric field that is perpendicular to the circular motion plane due to opposite contributions of different electrons.

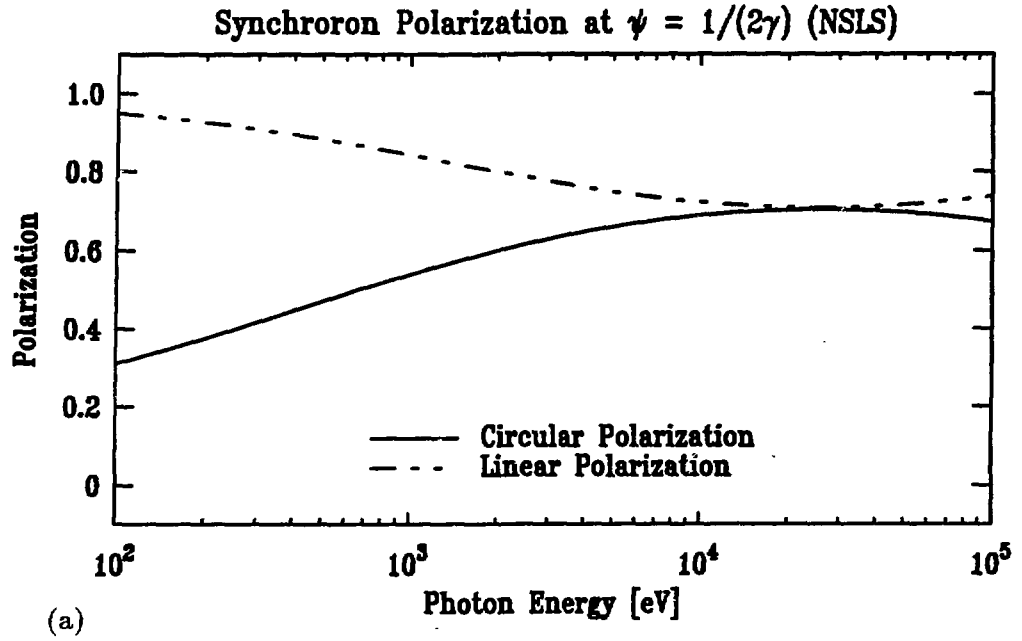

(a)

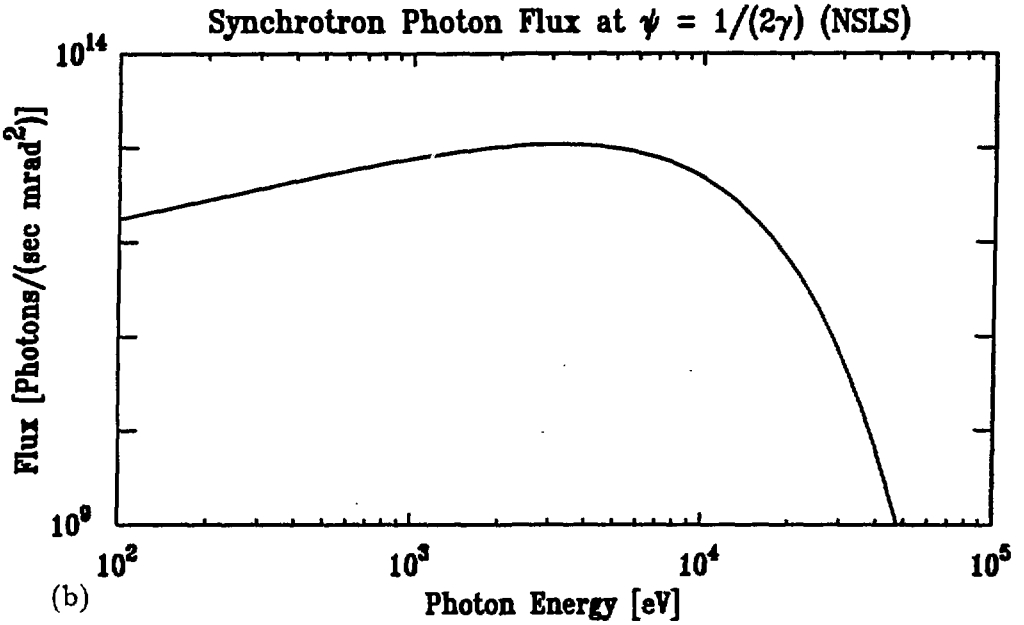

(b)

Figure 5: Properties of the synchrotron radiation from a bending magnet source at NSLS as a function of photon energy (a) linear and circular polarization (b) photon flux, for electron emittance $\epsilon_y = 2 \times 10^{-9}$m-rad, beta function $\beta_y = 16$m angular spread $\sigma_{y'} = 11\mu$rad.

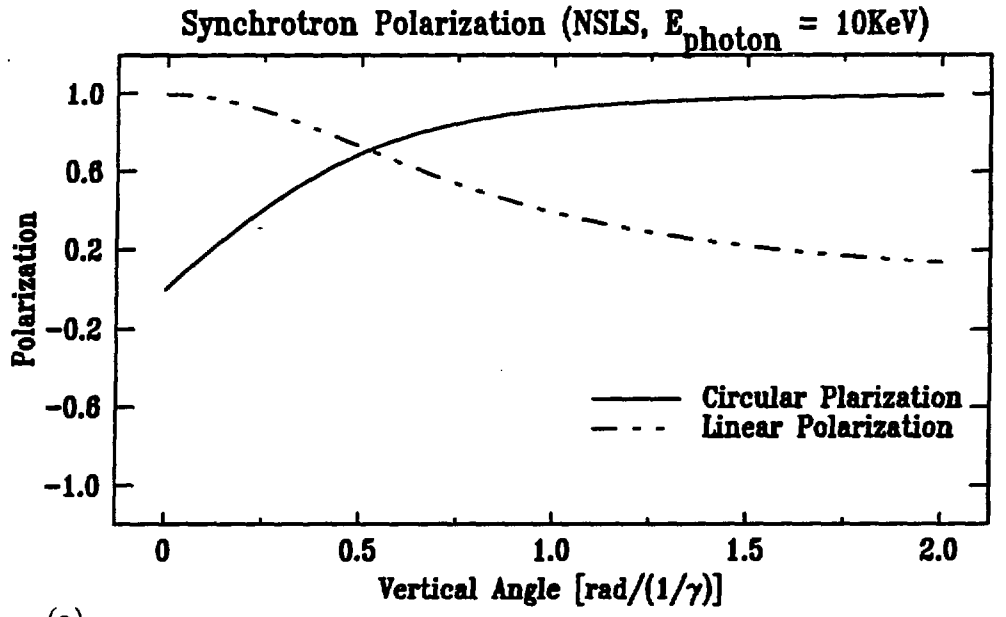

(a)

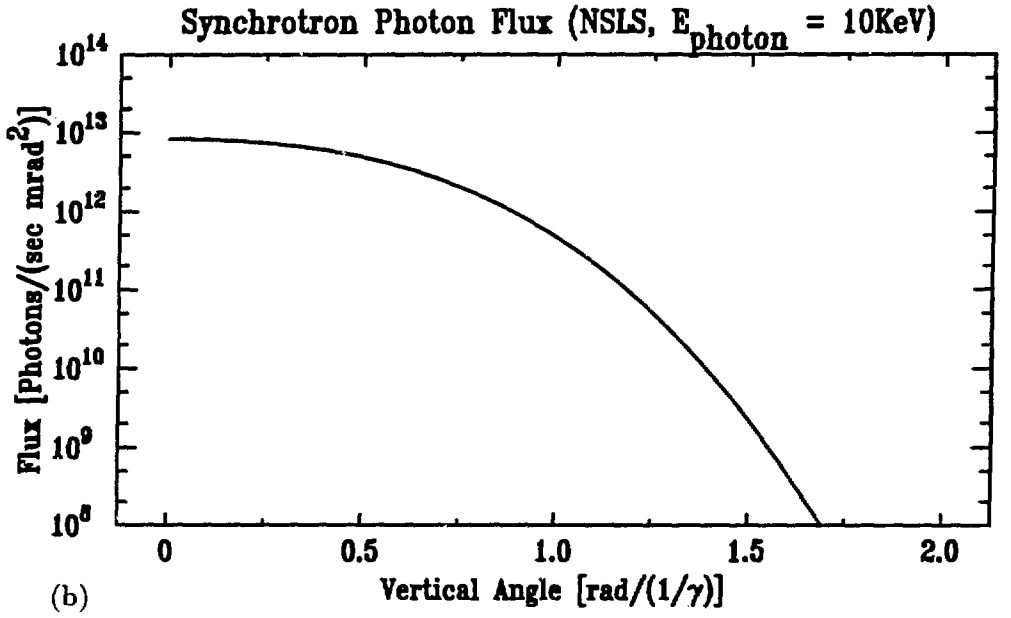

(b)

Figure 6: Properties of the synchrotron radiation at 10 KeV from a bending magnet source at NSLS as a function of vertical angle (a) polarization (b) photon flux, for angular spread $\sigma_{y'} = 11\mu$rad.

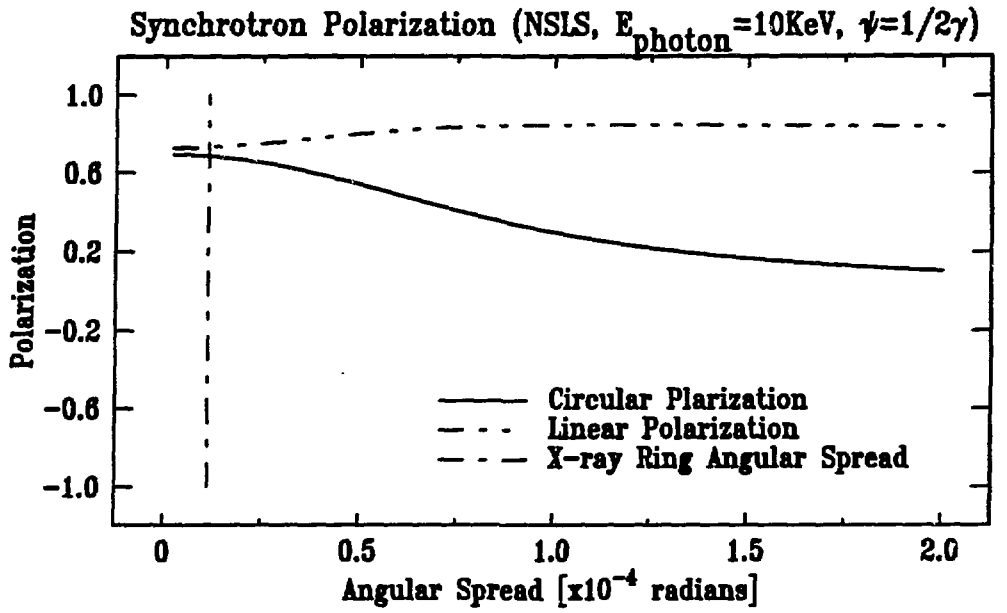

(a)

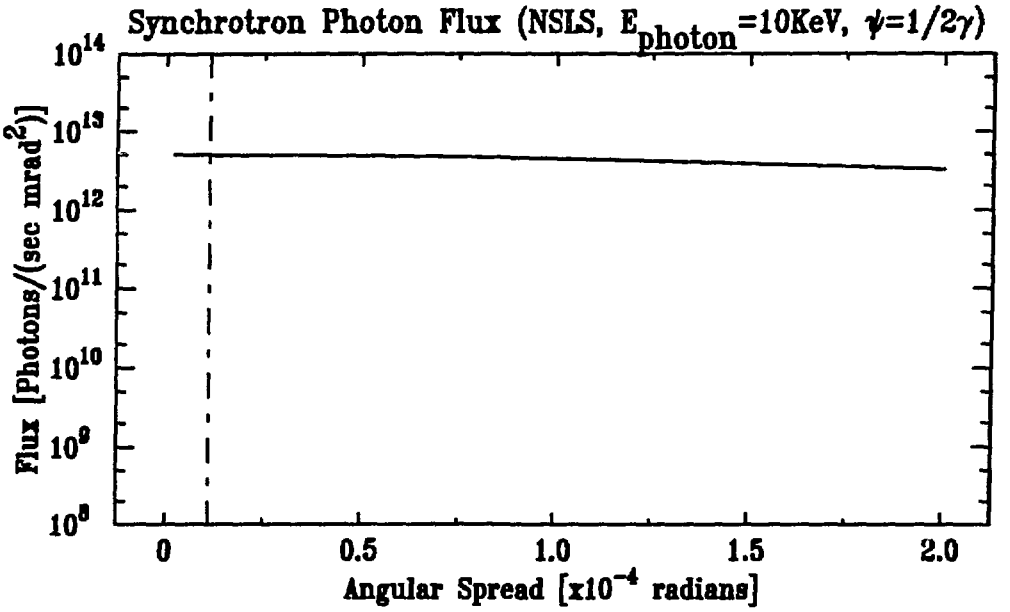

(b)

Figure 7: Dependance of synchrotron radiation (a) polarization (b) photon flux on the vertical spread of the electron beam, at 10KeV photon energy.

4. Elliptically Polarized Wiggler

Consider a wiggler magnet constructed from a vertical wiggler and a horizontal wiggler superimposed with a $\pi/2$ phase difference between them[6,7] (Fig. 2). The magnetic field on axis is:

$$\begin{aligned} B_y &= -\frac{2\pi mc}{e}\frac{K_y}{\lambda_w}\sin k_w z \\ B_x &= -\frac{2\pi mc}{e}\frac{K_x}{\lambda_w}\cos k_w z \end{aligned} \tag{22}$$

where λ_w is the wiggler period and $k_w \equiv 2\pi/\lambda_w$. The horizontal wiggler field is weaker than the vertical wiggler field ($K_x/K_y < 1$).

The radiation from an electron moving through this wiggler may be calculated by the methods presented in Section 2. This calculation was carried out using a computerized algebra program[15] and Saddle Point integration[16]. The results of the calculation were coded into a computer program that was used to generate the graphs in this section. An easier[6,7] approach can be used in order to get a rough estimate of the properties of the radiation that will also give some insight into the physics involved. For large K_y and photon energy close to the critical energy or higher, most of the radiation emanates from small sections of the electron trajectory around the tangent point to the viewing line. These sections, being very small, can be approximated as arcs with radii of curvature that can be calculated. The radiation is then calculated using the synchrotron radiation formulae. This is called the "*Bend Source*" approximation[6]. Note, that every wiggler period has two such points and their corresponding radii are opposite in sign (Fig. 8). In a planar wiggler, these two points will yield ΔW_θ which are equal in magnitude and opposite in sign. Thus, there is no circular polarization component to the Stokes vector. In an elliptical wiggler, these two arcs are at different angles to the viewer, resulting in a net circular polarization.

The radius of curvature of a curve is calculated by drawing a line that is perpendicular to the tangent to the curve, then moving an infinitesimal distance Δx and drawing another such line. The distance between the points where these lines cross each other and the curve is the radius (see Fig. 9). The radius calculated this way is

$$\rho = \frac{1}{y''}\left(1 + y'^2\right)^{3/2}. \tag{23}$$

The radius calculated for an electron in an elliptical wiggler is:

$$\rho = \lambda_w \left(1 + \xi^2\right)^{3/2} \frac{\gamma}{2\pi\sqrt{K_y^2 - \gamma^2\xi^2}}. \tag{24}$$

where ξ is the projection of the angle between the wiggler axis and the target of the radiation into the x-z plane. The vertical angles between the viewer and the arcs are:

$$\begin{aligned} \psi_+ &= \psi + \frac{K_x}{\gamma} \\ \psi_- &= \psi - \frac{K_x}{\gamma} \end{aligned} \tag{25}$$

Inserting Eqs. 24, 25 into Eqs. 18, one finds the radiation parameters on axis ($\psi = \xi = 0$) in the bend source approximation[6]:

$$\begin{aligned} \Delta W_\theta &= \sqrt{\frac{2}{3}} \frac{K_x\sqrt{1+K_x^2}}{\gamma K_y} \frac{\lambda_w}{\pi} K_{1/3}(\eta_0) \\ \Delta W_\xi &= -i\sqrt{\frac{2}{3}} \frac{1+K_x^2}{\gamma K_y} \frac{\lambda_w}{\pi} K_{2/3}(\eta_0) \\ \eta_0 &= \frac{\omega}{2\omega_c}\left(1+K_x^2\right)^{3/2} \\ \omega_c &= \frac{3\pi c\gamma^2 K_y}{\lambda_w} \end{aligned} \tag{26}$$

demonstrating that elliptical wigglers generate circularly polarized light on-axis[6,7]. Figs. 10–12 show the photon flux and polarization that can be produced by elliptical wigglers in NSLS X-ray ring straight sections ($\epsilon_y = 2 \times 10^{-9}$m, $\beta_y = 30$cm, $\sigma_{y'} = 80\mu$rad). The fluxes are computed per wiggler period and should be multiplied by the total number of periods in the wiggler. Note that the flux peaks at a vertical angle of about $\psi = K_x/\gamma$ where the circular polarization is zero. The net flux of circularly polarized photons peaks at about $\psi = 0.75K_x/\gamma$ (Fig. 12) which is, therefore, a recommended working angle. Since the polarization criteria are symmetric around $\psi = 0$, a measurement of the polarization can be taken at $\psi = -\psi_{max}$ at the same time the experiment is performed at $\psi = \psi_{max}$

(ψ_{max} being the angle at which the flux of circularly polarized photons is maximum). This method will also detect sudden changes of the electron beam position and their effect on the polarization. There is a trade off between the polarization and the flux on axis. A higher K_x value will yield a higher degree of circular polarization, but will decrease the photon flux on axis significantly. This is due to the fact that for large K_x the angle between the two bends in a period becomes larger, thus producing less radiation on axis. Note, however, that for each K_x the maximum circularly polarized photon flux is comparable. Hence, the angle of the experiment can be tailored to the value of K_x chosen.

Figs. 13 show the polarization as a function of the electron beam vertical angular spread for various observation angles. The results are somewhat surprising in that the reduction in circular polarization is not as drastic as expected. The physical explanation for this is that there are two bends (in each period) contributing to the circular polarization and electrons that have large angle will still produce significant circular polarization from one of the bends. Figs. 13g,13h demonstrates that when choosing an observation angle in which the polarized photon flux is maximal for given K_x, the effect of the angular spread is minimal. For completeness of the study we are also presenting Figs. 14 which are the corresponding photon fluxes. Note that for $K_x = 1$, the photon flux does not change drastically as a function of angular spread.

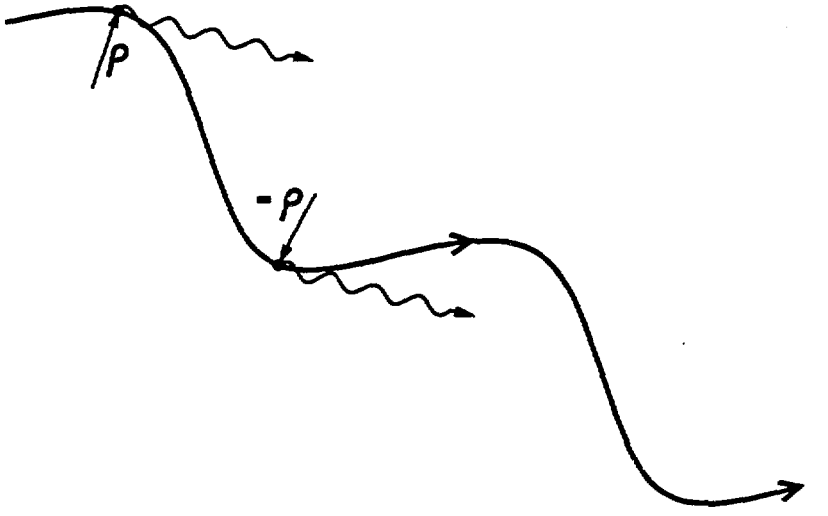

Figure 8: Bend Source approximation

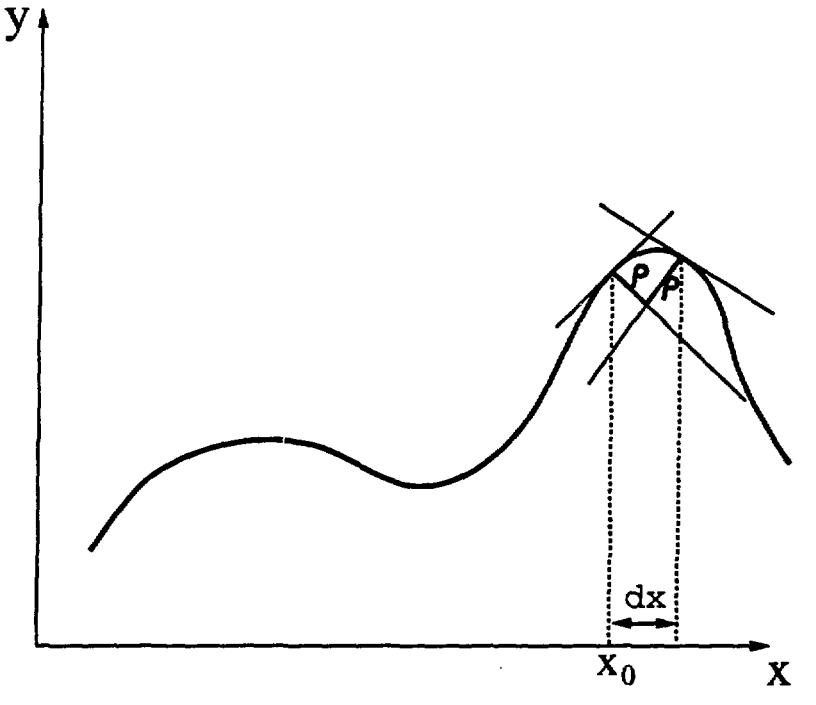

Figure 9: Finding the local radius of a curve

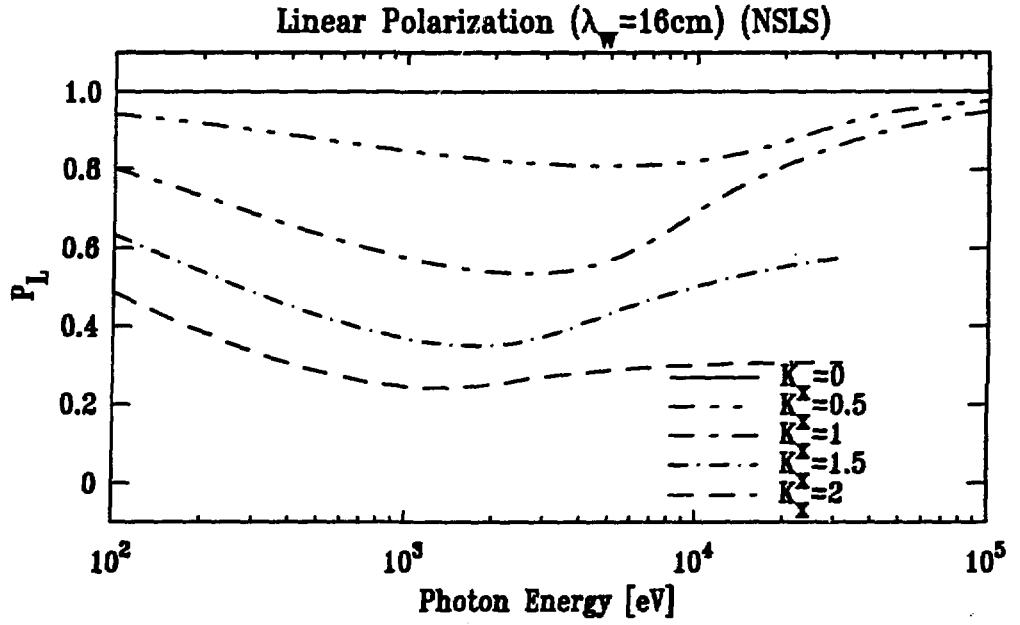
Linear Polarization (λ_w=16cm) (NSLS)
1.0
0.8
0.6
0.4
0.2
0
P_L
K_x=0
K_x=0.5
K_x=1
K_x=1.5
K_x=2
10^2
10^3
10^4
10^5
Photon Energy [eV]

(a)

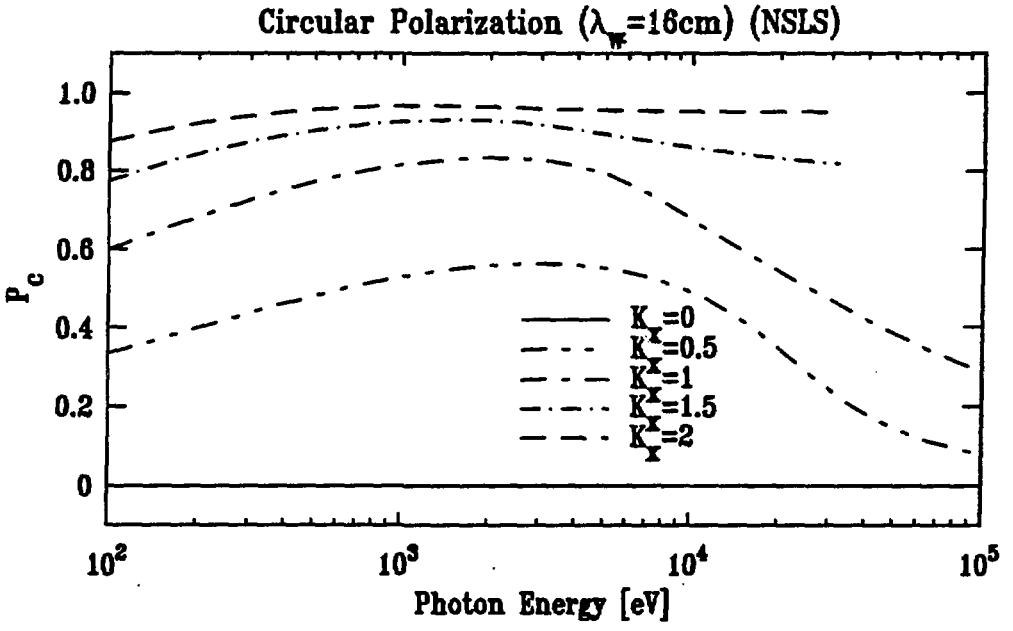
Circular Polarization (λ_w=16cm) (NSLS)
1.0
0.8
0.6
0.4
0.2
0
P_c
K_x=0
K_x=0.5
K_x=1
K_x=1.5
K_x=2
10^2
10^3
10^4
10^5
Photon Energy [eV]

(b)

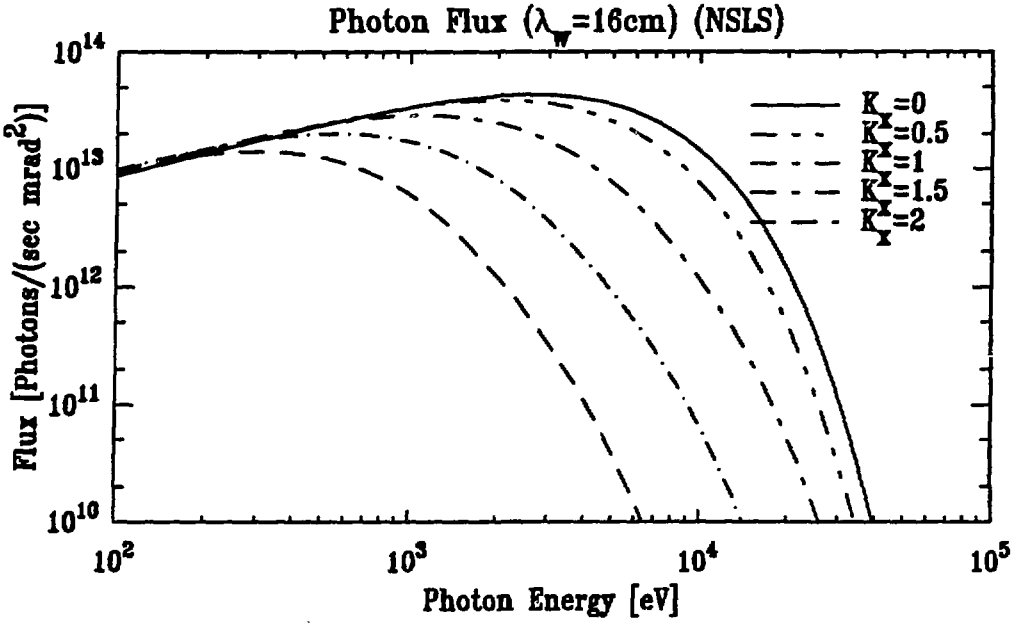

(c)

Figure 10: On axis (a) Linear polarization of elliptical wigglers as a function of photon energy, (b) circular polarization, (c) photon flux per period [$K_y = 13$, $I = 200$mAmp, $\Delta\lambda/\lambda = 10^{-3}$].

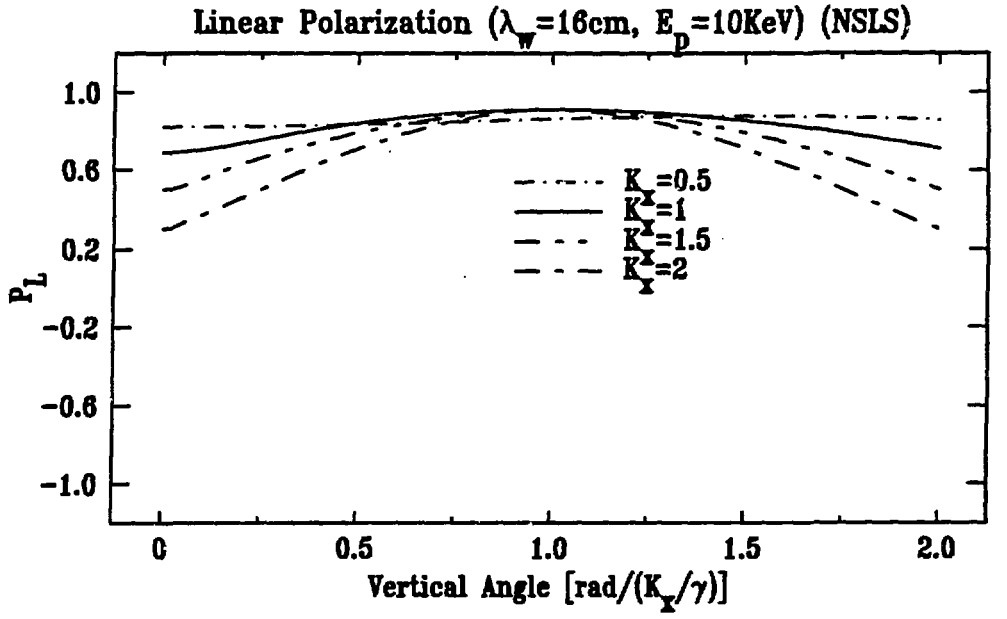

(a)

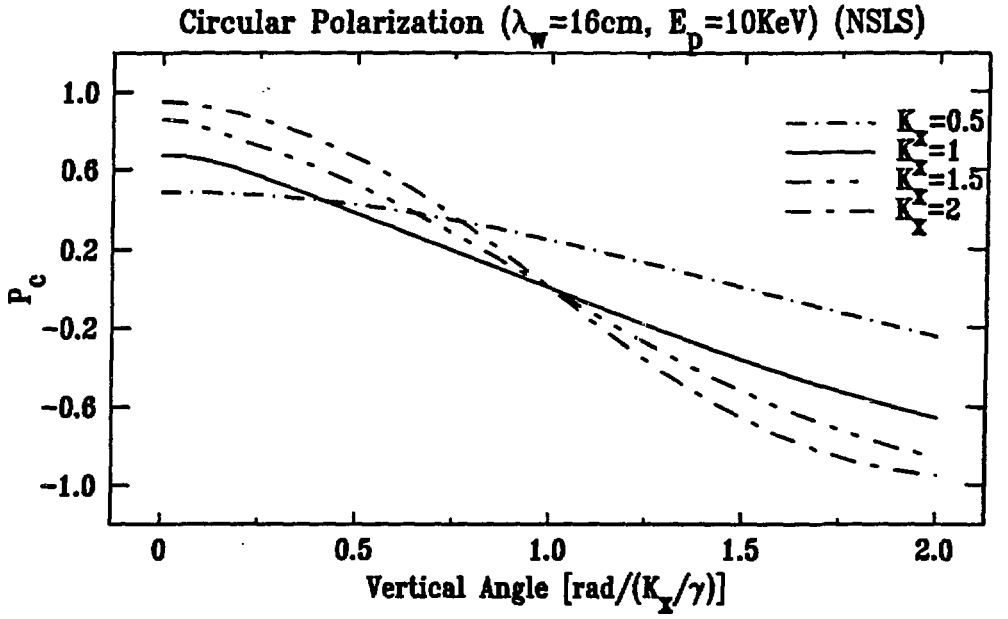

(b)

Figure 11: Polarization as a function of vertical angle (a) linear polarization (b) circular polarization [$K_y = 13$, $I = 200$mAmp, $\Delta\lambda/\lambda = 10^{-3}$].

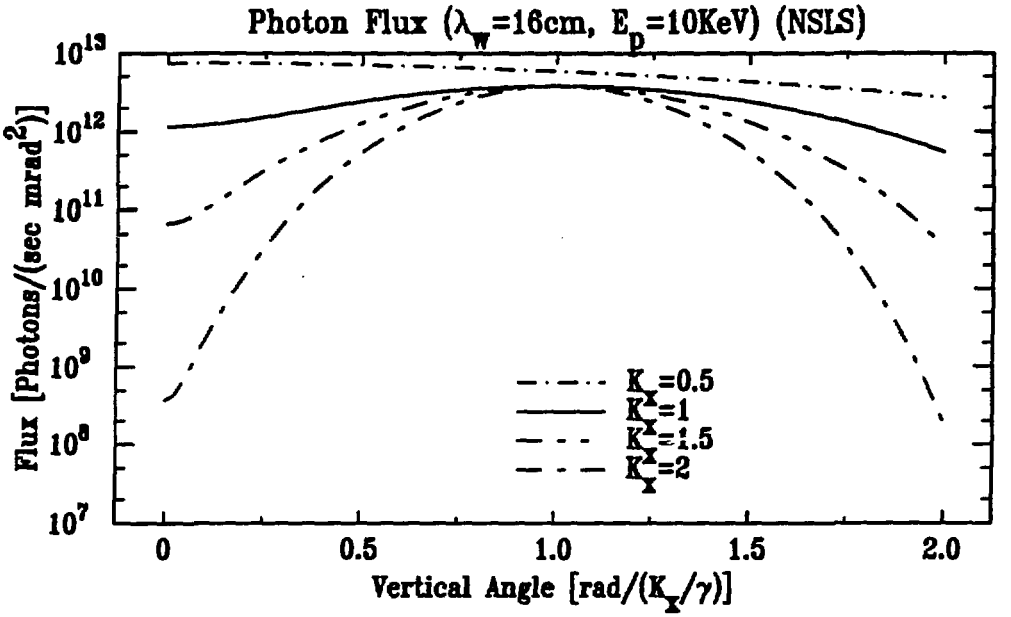

(a)

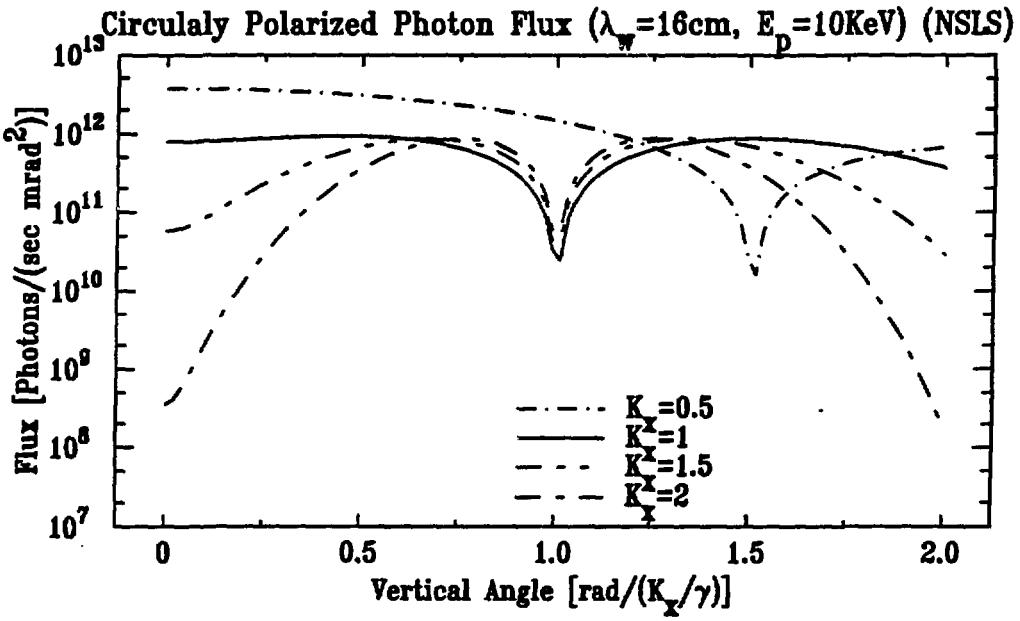

(b)

Figure 12: Photon flux as a function of vertical angle (a) total flux per period (b) net circularly polarized flux per period [$K_y = 13$, $I = 200$mAmp, $\Delta\lambda/\lambda = 10^{-3}$].

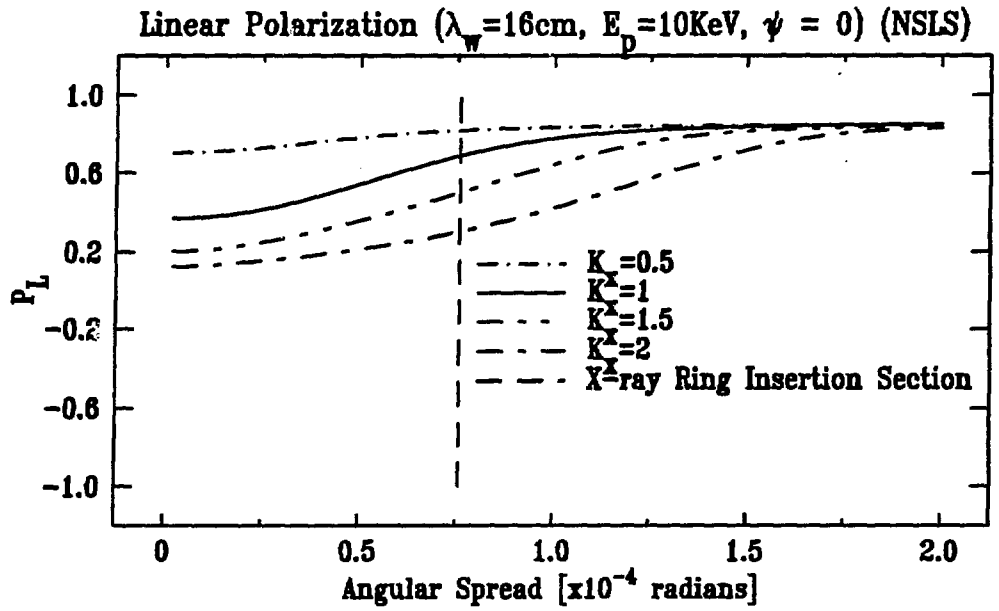
Linear Polarization (λ_w=16cm, E_p=10KeV, ψ = 0) (NSLS)
1.0
0.6
0.2
-0.2
-0.6
-1.0
P_L
0
0.5
1.0
1.5
2.0
Angular Spread [x10^{-4} radians]
K_x=0.5
K_x=1
K_x=1.5
K_x=2
X-ray Ring Insertion Section

(a)

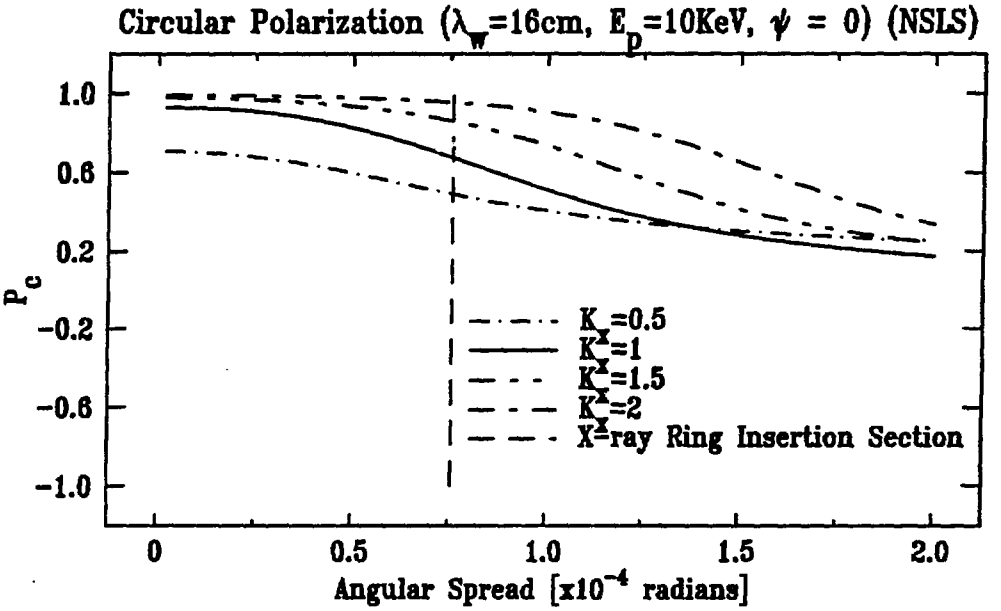
Circular Polarization (λ_w=16cm, E_p=10KeV, ψ = 0) (NSLS)
1.0
0.6
0.2
-0.2
-0.6
-1.0
P_c
0
0.5
1.0
1.5
2.0
Angular Spread [x10^{-4} radians]
K_x=0.5
K_x=1
K_x=1.5
K_x=2
X-ray Ring Insertion Section

(b)

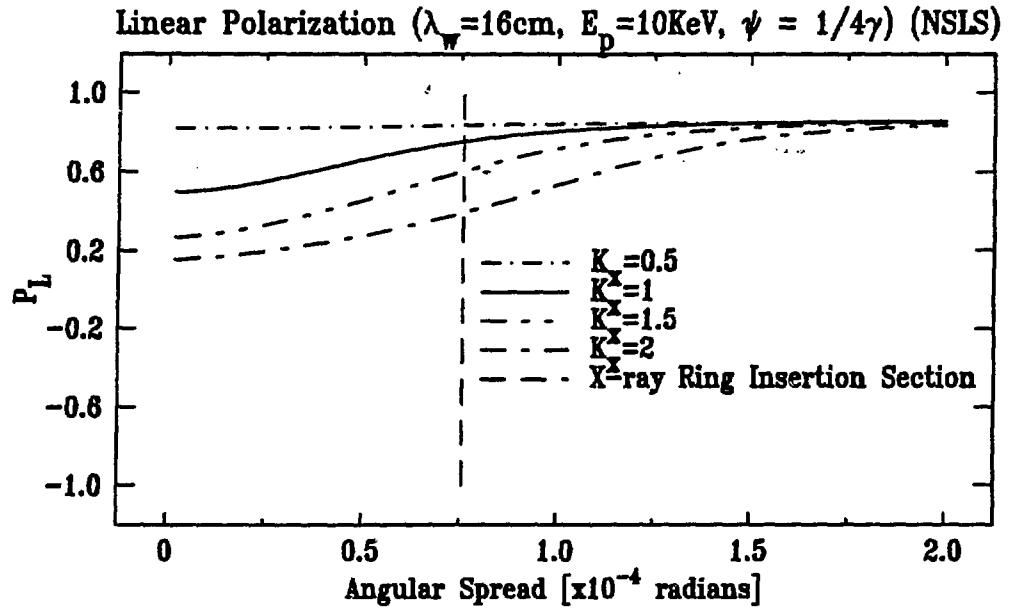
Linear Polarization (λ_w=16cm, E_p=10KeV, ψ = 1/4γ) (NSLS)
1.0
0.6
0.2
-0.2
-0.6
-1.0
P_L
0
0.5
1.0
1.5
2.0
Angular Spread [x10^{-4} radians]
K_x=0.5
K_x=1
K_x=1.5
K_x=2
X-ray Ring Insertion Section

(c)

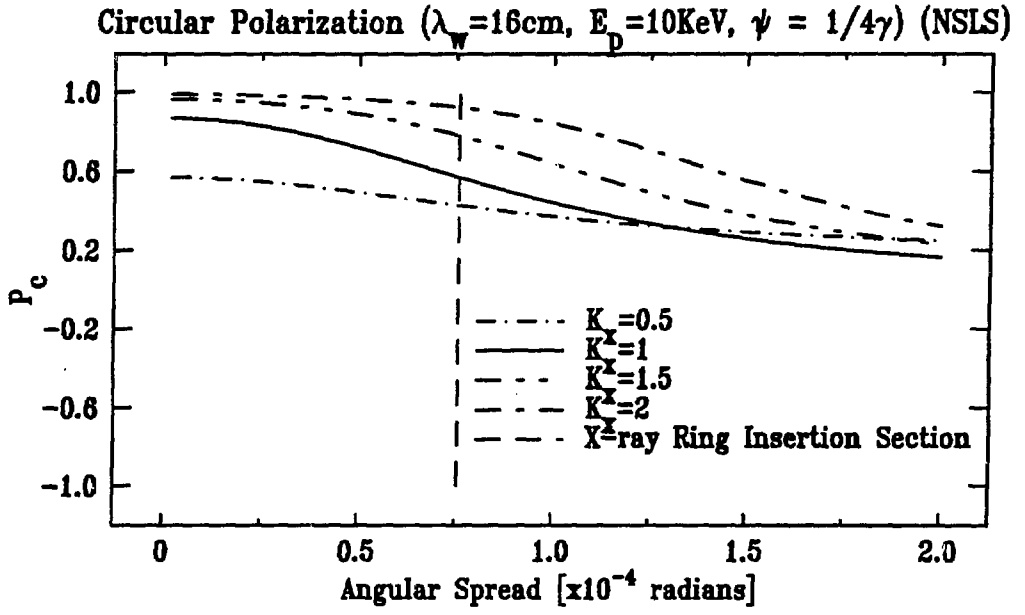
Circular Polarization (λ_w=16cm, E_p=10KeV, ψ = 1/4γ) (NSLS)
1.0
0.6
0.2
-0.2
-0.6
-1.0
P_c
0
0.5
1.0
1.5
2.0
Angular Spread [x10^{-4} radians]
K_x=0.5
K_x=1
K_x=1.5
K_x=2
X-ray Ring Insertion Section

(d)

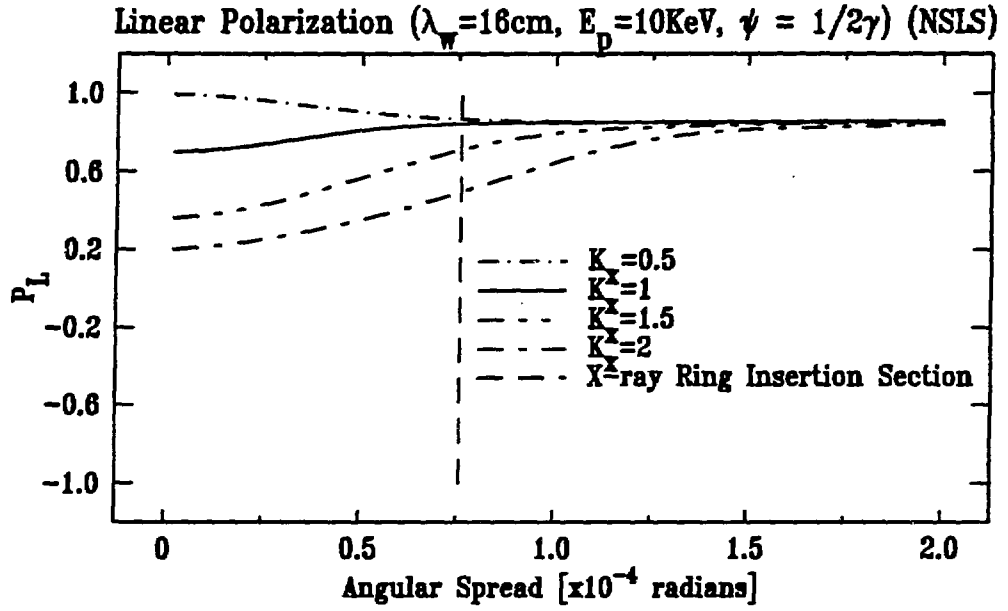
Linear Polarization (λ_w=16cm, E_p=10KeV, ψ = 1/2γ) (NSLS)
1.0
0.6
0.2
-0.2
-0.6
-1.0
P_L
0
0.5
1.0
1.5
2.0
Angular Spread [x10^{-4} radians]
K_x=0.5
K_x=1
K_x=1.5
K_x=2
X-ray Ring Insertion Section

(e)

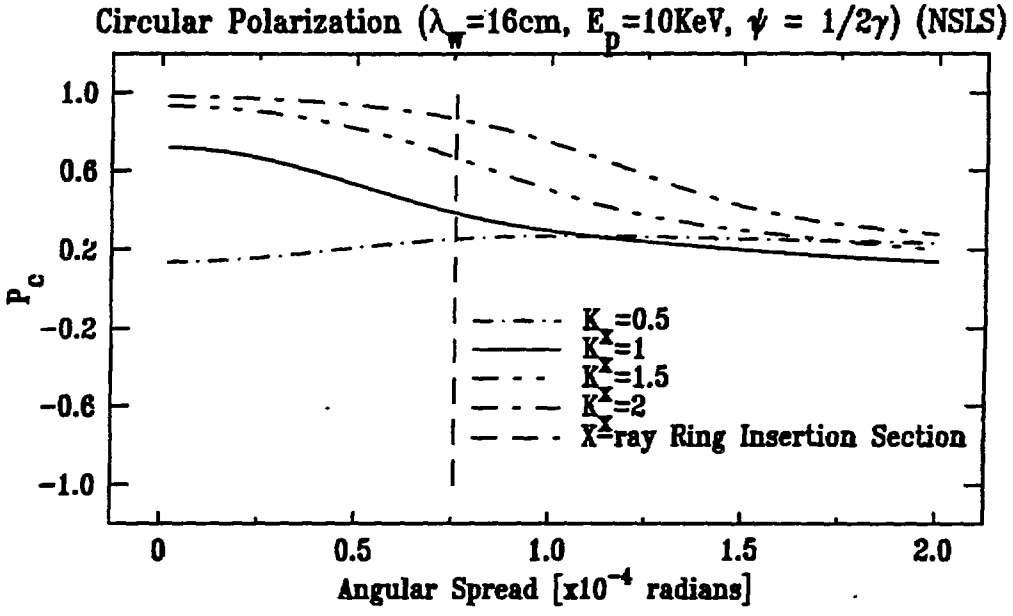
Circular Polarization (λ_w=16cm, E_p=10KeV, ψ = 1/2γ) (NSLS)
1.0
0.6
0.2
-0.2
-0.6
-1.0
P_c
0
0.5
1.0
1.5
2.0
Angular Spread [x10^{-4} radians]
K_x=0.5
K_x=1
K_x=1.5
K_x=2
X-ray Ring Insertion Section

(f)

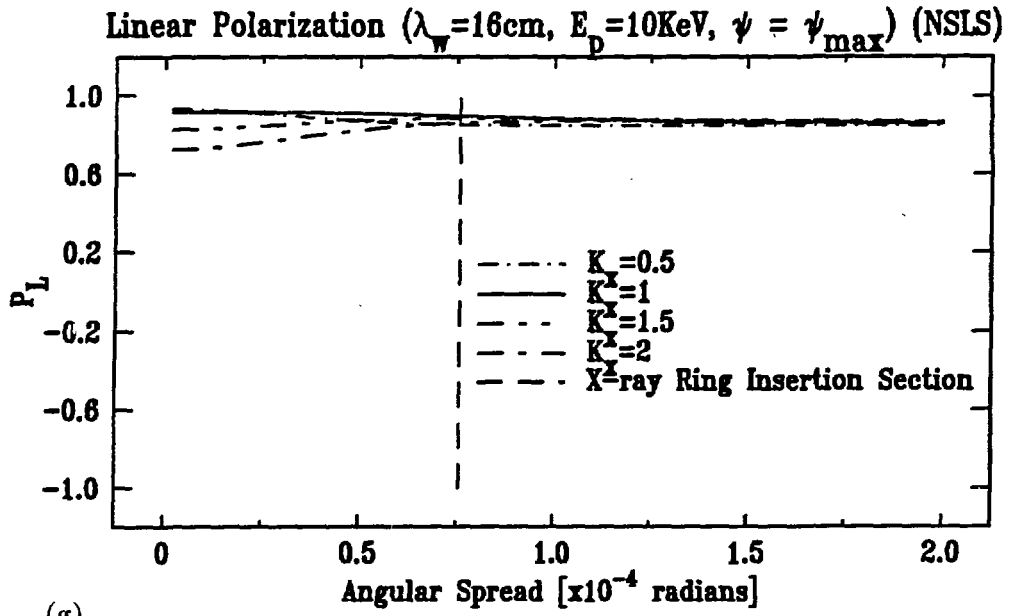

(g)

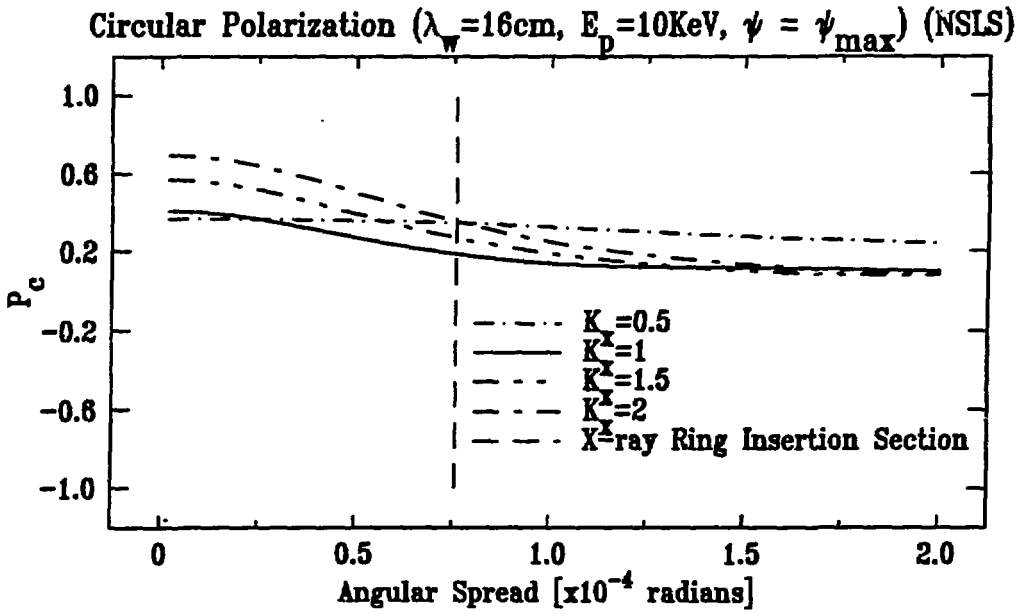

(h)

Figure 13: Polarization as a function of electron beam vertical angular spread. (a) Linear polarization, $\psi = 0$, (b) Circular polarization, $\psi = 0$, (c) Linear polarization, $\psi = 1/4\gamma$, (d) Circular polarization, $\psi = 1/4\gamma$, (e) Linear polarization, $\psi = 1/2\gamma$, (f) Circular polarization, $\psi = 1/2\gamma$, (g) Linear polarization, $\psi = \psi_{max}$, (h) Circular polarization, $\psi = \psi_{max}$ [$K_y = 13$, $I = 200$mAmp, $\Delta\lambda/\lambda = 10^{-3}$].

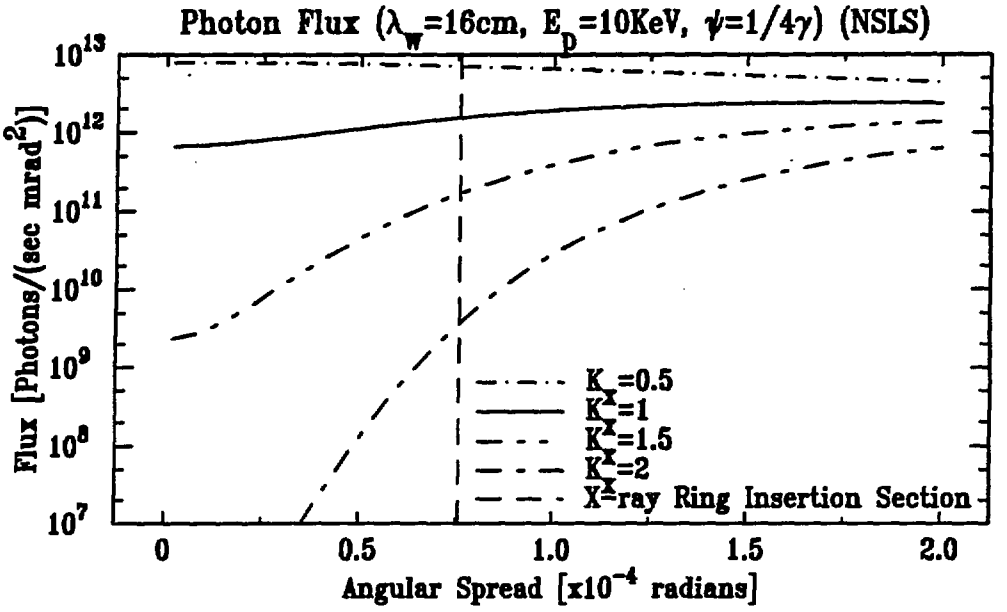
Photon Flux (λ_w=16cm, E_p=10KeV, ψ=1/4γ) (NSLS)
Flux [Photons/(sec mrad^2)]
10^{13}
10^{12}
10^{11}
10^{10}
10^{9}
10^{8}
10^{7}
0
0.5
1.0
1.5
2.0
Angular Spread [x10^{-4} radians]
K_x=0.5
K_x=1
K_x=1.5
K_x=2
X-ray Ring Insertion Section

(c)

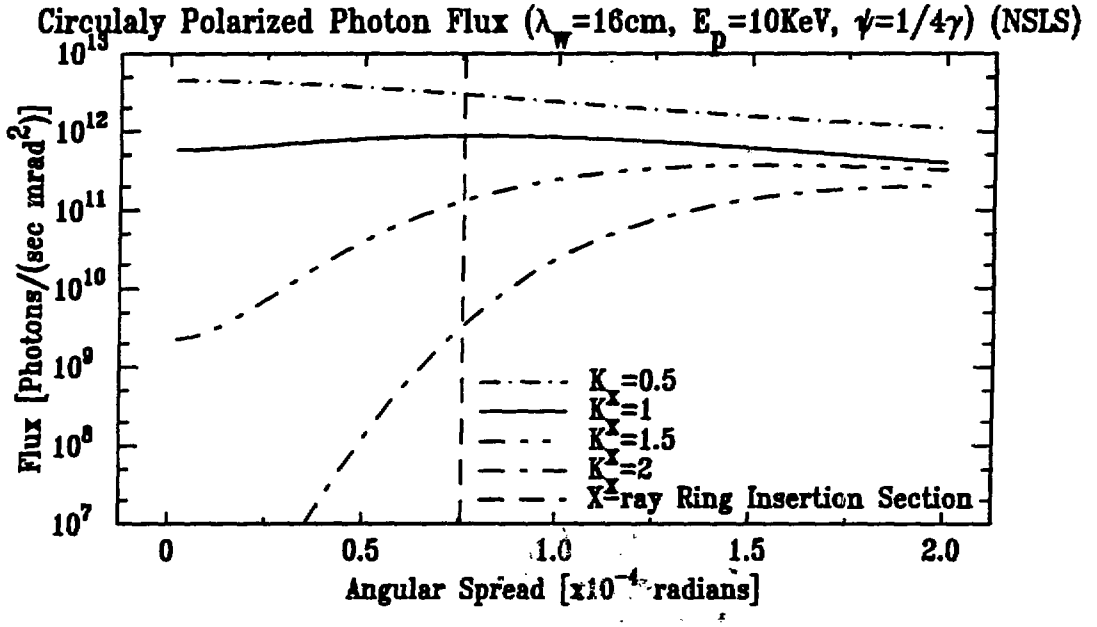
Circulaly Polarized Photon Flux (λ_w=16cm, E_p=10KeV, ψ=1/4γ) (NSLS)
Flux [Photons/(sec mrad^2)]
10^{13}
10^{12}
10^{11}
10^{10}
10^{9}
10^{8}
10^{7}
0
0.5
1.0
1.5
2.0
Angular Spread [x10^{-4} radians]
K_x=0.5
K_x=1
K_x=1.5
K_x=2
X-ray Ring Insertion Section

(d)

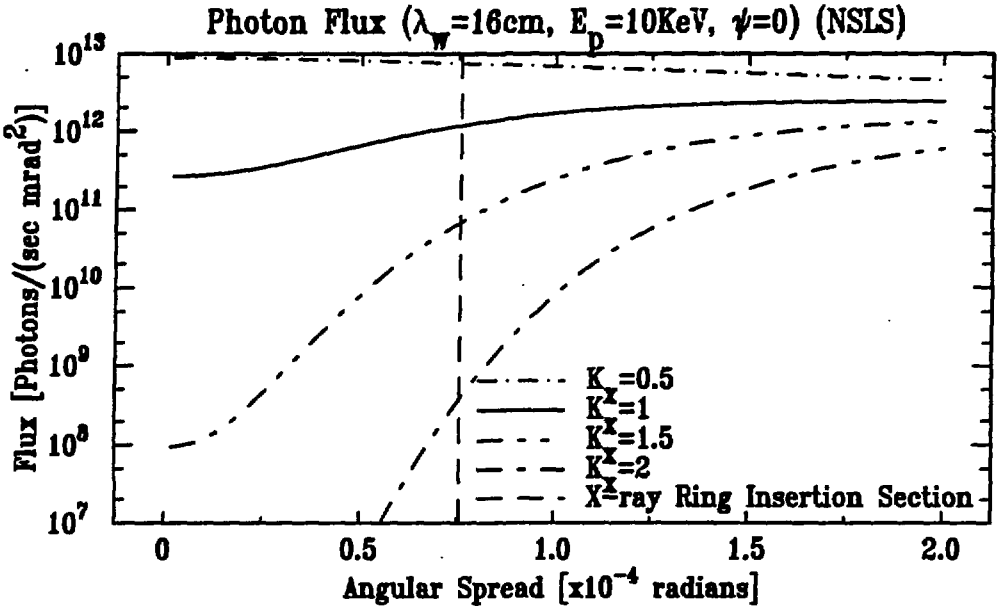
Photon Flux (λ_w=16cm, E_p=10KeV, ψ=0) (NSLS)
Flux [Photons/(sec mrad^2)]
10^{13}
10^{12}
10^{11}
10^{10}
10^{9}
10^{8}
10^{7}
0
0.5
1.0
1.5
2.0
Angular Spread [x10^{-4} radians]
K_x=0.5
K_x=1
K_x=1.5
K_x=2
X-ray Ring Insertion Section

(a)

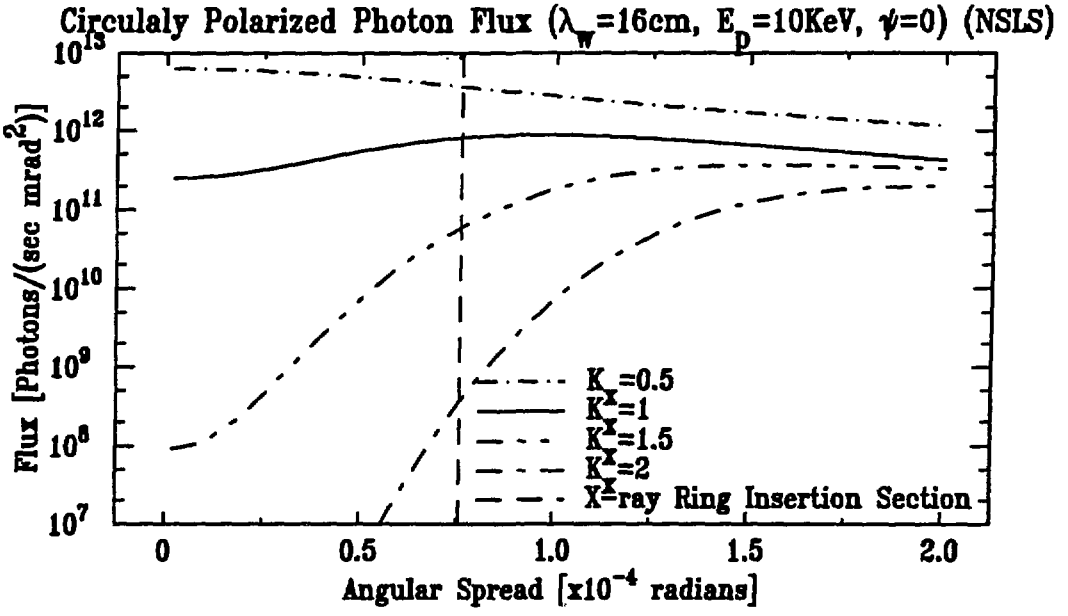
Circulaly Polarized Photon Flux (λ_w=16cm, E_p=10KeV, ψ=0) (NSLS)
Flux [Photons/(sec mrad^2)]
10^{13}
10^{12}
10^{11}
10^{10}
10^{9}
10^{8}
10^{7}
0
0.5
1.0
1.5
2.0
Angular Spread [x10^{-4} radians]
K_x=0.5
K_x=1
K_x=1.5
K_x=2
X-ray Ring Insertion Section

(b)

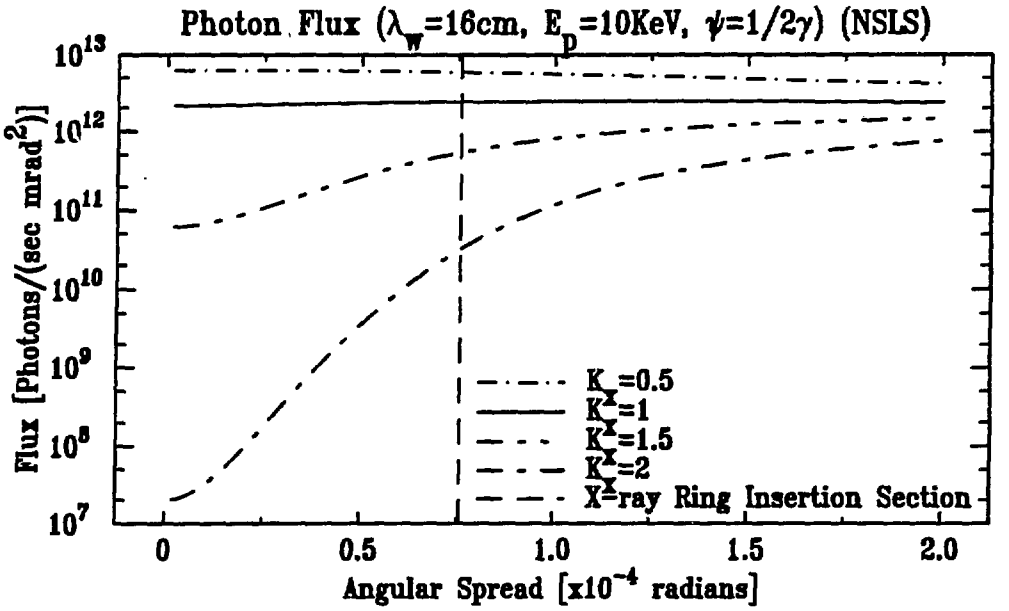
Photon Flux (λ_w=16cm, E_p=10KeV, ψ=1/2γ) (NSLS)
Flux [Photons/(sec mrad^2)]
10^{13}
10^{12}
10^{11}
10^{10}
10^{9}
10^{8}
10^{7}
0
0.5
1.0
1.5
2.0
Angular Spread [x10^{-4} radians]
K_x=0.5
K_x=1
K_x=1.5
K_x=2
X-ray Ring Insertion Section

(e)

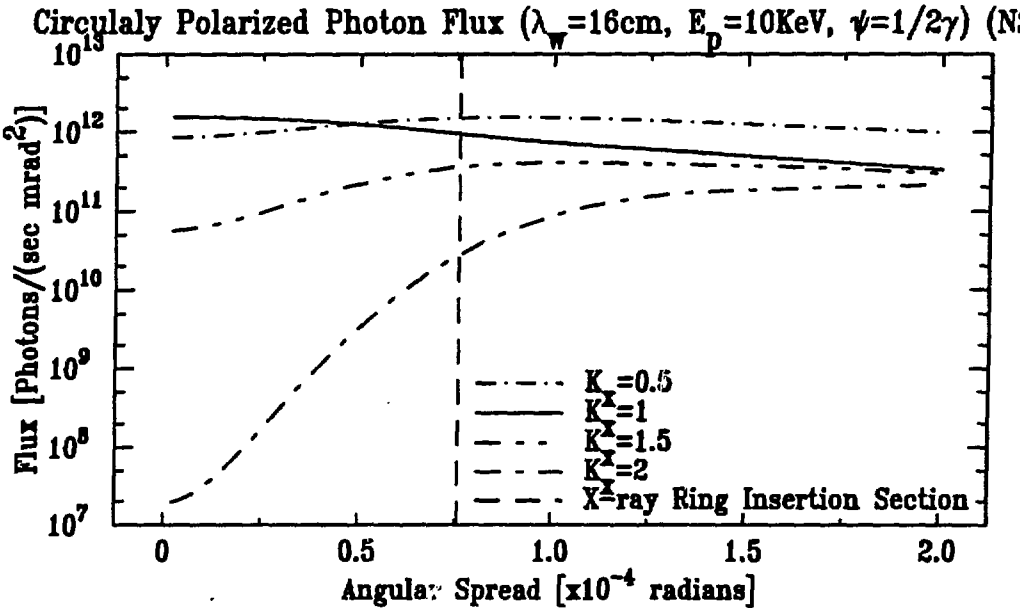
Circulaly Polarized Photon Flux (λ_w=16cm, E_p=10KeV, ψ=1/2γ) (NSLS)
Flux [Photons/(sec mrad^2)]
10^{13}
10^{12}
10^{11}
10^{10}
10^{9}
10^{8}
10^{7}
0
0.5
1.0
1.5
2.0
Angular Spread [x10^{-4} radians]
K_x=0.5
K_x=1
K_x=1.5
K_x=2
X-ray Ring Insertion Section

(f)

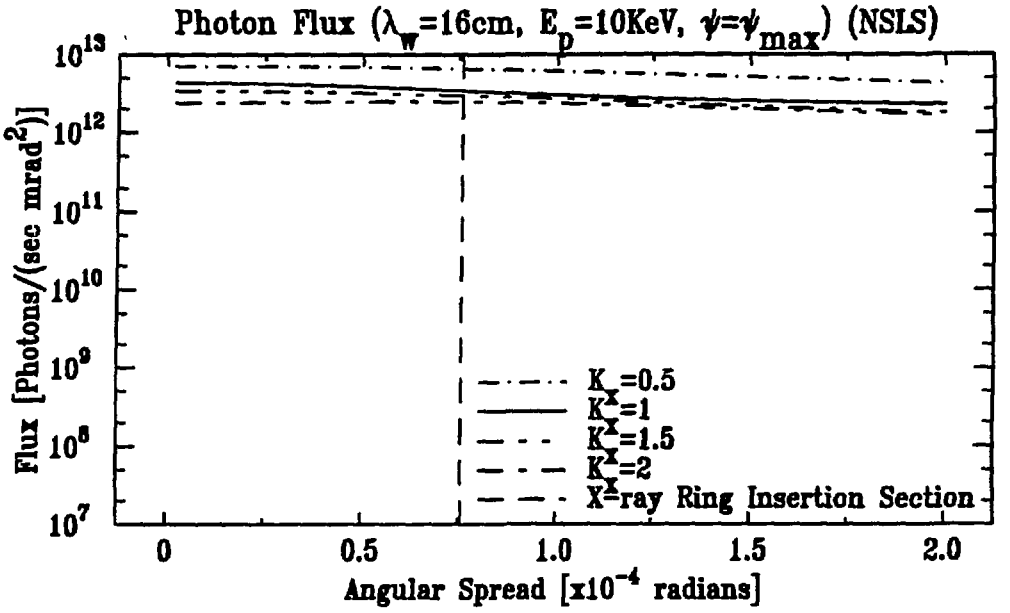

(g)

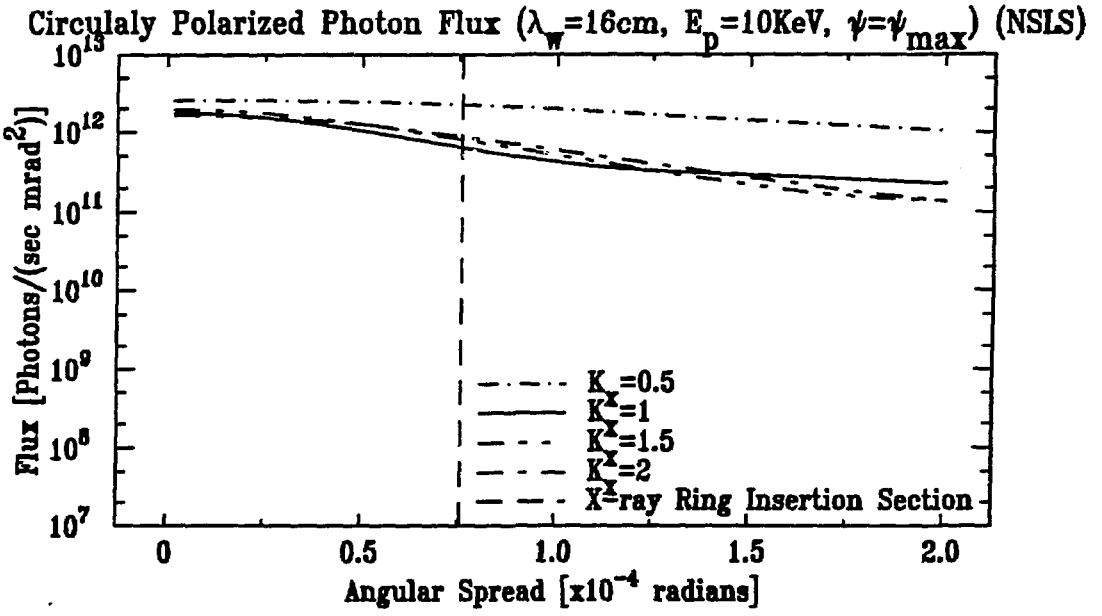

(h)

Figure 14: Photon flux per wiggler period as a function of electron beam vertical angular spread [$K_y = 13$, $I = 200$mAmp, $\Delta\lambda/\lambda = 10^{-3}$].

5. Conceptual Designs for Elliptical Wigglers

In all the designs discussed in this section the vertical wiggler is built from permanent magnet. Its realization is straightforward since the vertical gap is small and the desired value of $K_y = 13$ is easily achieved in a configuration with static horizontal field. The horizontal wiggler has a gap in the 6 to 8 cm range. An electromagnetic horizontal wiggler is of interest, so that the polarization can be modulated. In addition, if it is possible to move the horizontal wiggler relative to the vertical wiggler, we could also provide a source with a time-dependent linear polarization.

In a configuration with an AC horizontal wiggler there is a problem of eddy currents developing in the permanent magnet material. To solve this problem, it is necessary to use a high resistivity permanent magnet, such as epoxy bound materials. However, the maximum remnant field that is achieved in these materials is only about 6KGauss (private communication with K. Halbach). This will yield only $K_y = 11$ in the configuration discussed. Consequently the photon spectrum will be softer than what was presented here.

5.1. Permanent magnet horizontal wiggler

The magnetic field of a permanent magnet wiggler on axis is given by[8]:

$$B_0 = 2B_r \frac{\sin \pi/M}{\pi/M} \left(1 - e^{-2\pi h/\lambda_w}\right) e^{-\pi g/\lambda_w} \tag{27}$$

where B_r is the remnant field in the magnet, M is the number of blocks per period, h is the height of a block, and g is the wiggler gap. We choose to use a conservative value for B_r (0.8 T), $M = 4$ and $h = \lambda_w/4$. Table 1 shows the calculated wiggler strength on axis for $\lambda_w = 12$ cm and $\lambda_w = 16$ cm. Two gap sizes are examined; $g = 8$ cm and $g = 10$ cm. Only small values of K can be achieved when $\lambda_w = 12$ cm. Better values of K are obtained with 16 cm period.

Table 1: Permanent Horizontal Wiggler Parameters

	$\lambda_w = 12$ cm	$\lambda_w = 16$ cm
$g = 10$ cm	$B_0 = 0.083$ T; $K = 0.93$	$B_0 = 0.16$ T; $K = 2.393$
$g = 8$ cm	$B_0 = 0.14$ T; $K = 1.57$	$B_0 = 0.24$ T; $K = 3.54$

5.2. Air core electromagnetic horizontal wiggler

An air core electromagnet excited with AC has the virtues that it does not have eddy currents in its core, and that it is linear throughout its cycle. Thus, beam dynamics are more easily understood and handled. Table 2 shows the parameters of an air core electromagnetic wiggler with $K_x = 1$ and $\lambda_w = 16$ cm (see Fig. 15). Three gap sizes are examined. To calculate these parameters we used Eq. 27 (with $M = 2$), but this time B_r represents the field in the coil.

$$\begin{aligned} B_r &= \mu_0 H \\ H &= J\, D \end{aligned} \tag{28}$$

were D is the width of the coils (in our example $D = 3$ cm). The current densities required are achievable. However, water cooling will be necessary.

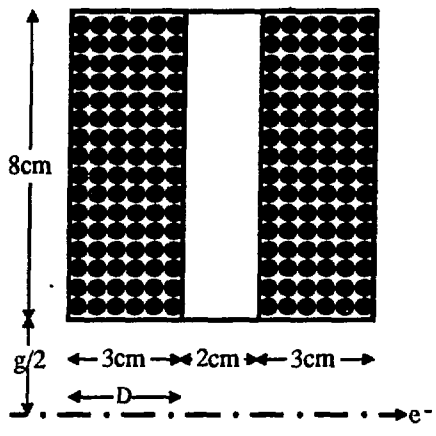

Figure 15: Air core magnet configuration

Table 2: Air Core Electromagnetic Wiggler Parameters ($\lambda_w = 16$cm, $K_x = 1$)

g[cm]	8	6	4
B_0/B_r	0.2532	0.375	0.555
$B_r[KGauss]$	2.64	1.78	1.21
$J[KAmp/\text{cm}^2]$	0.7	0.47	0.32

5.3. Iron core electromagnetic horizontal wiggler

An iron core electromagnet has the advantage that the current required is much lower than that of an air core electromagnet. The problem of eddy currents may be alleviated by using laminated iron. The use of transformer iron which contains silicon, will further reduce the generation of eddy currents. A typical configuration of an iron core electromagnetic wiggler[9,10] is shown in Fig. 16. In reference 9 Halbach developed an algorithm for optimizing such a configuration. We present here only the final results of this algorithm. The total flux entering the pole and leaving at the top is:

$$B_2 W = B_0 W f_2 + \mu_0 J D_2^2 \tag{29}$$

where B_2 is the maximum field allowed in the iron, B_0 is the corresponding field on axis, $f_2 > 1$ accounts for the variation of the field along the bottom of the pole, and J is the current density. The field on axis is[9,10]:

$$\begin{aligned} B_0 &= \frac{B_2}{f_2} \frac{2}{1+\sqrt{1+16B_2/b}} \\ b &= 4\mu_0 J W \left(\frac{D_1}{g}\right)^2 \left(\frac{f_2}{f_1}\right)^2 \end{aligned} \tag{30}$$

where $f_1 > 1$ accounts for the change in the field between the wiggler axis and the wiggler tip. f_1 and f_2 are, usually, weakly dependent on the geometry. Table 3 shows calculation of the various parameters for a wiggler with $\lambda_w = 16$ cm, and $D_1/\lambda_w = 0.2875$. The corresponding f's are $f_1 \approx 1.17$ and $f_2 \approx 2.35$. We limited the field in the iron to $B \leq 1$ Tesla in order to use transformer iron, and the current density to 200 Amp/cm^2 in order to use air cooled coils. Two gap sizes are examined. The second row in Table 3 represents the field on axis with $J = 200$ Amp/cm^2. The fourth row represents the current density

required for $K_x = 1$.

Table 3: Iron Core Electromagnetic Wiggler Parameters ($\lambda_w = 16$cm)

	$g = 6$ cm	$g = 8$ cm
$B_{0_{max}}$ [Tesla] ($J = 200$Amp/cm^2)		
	0.1532	0.1214
J [Amp/cm^2]	87.32	110.2

The design with $g = 8$ cm requires a current density of 110 Amp/cm^2 which is well under the limit for air cooled coil.

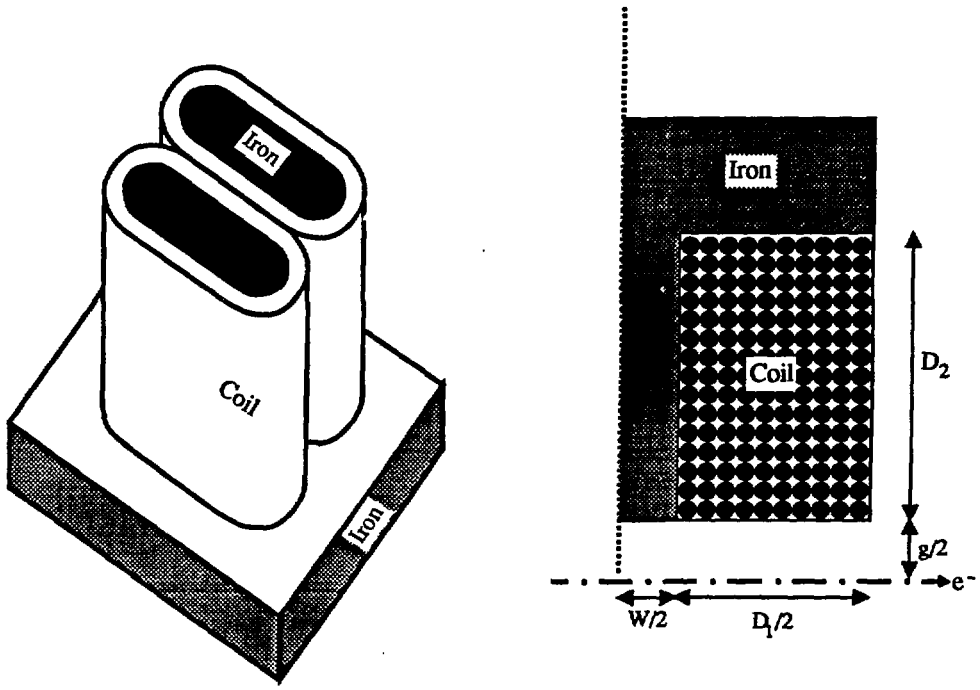

Figure 16: Iron core magnet configuration

A Poisson run (Figs. 17) reveals that the degradation of the permanent magnet field due to the proximity of the iron is insignificant. This concept seems to be viable for the realization of an AC elliptical wiggler[11]. However, further simulation is necessary in order to determine the three dimensional field structure and the effects of the eddy currents.

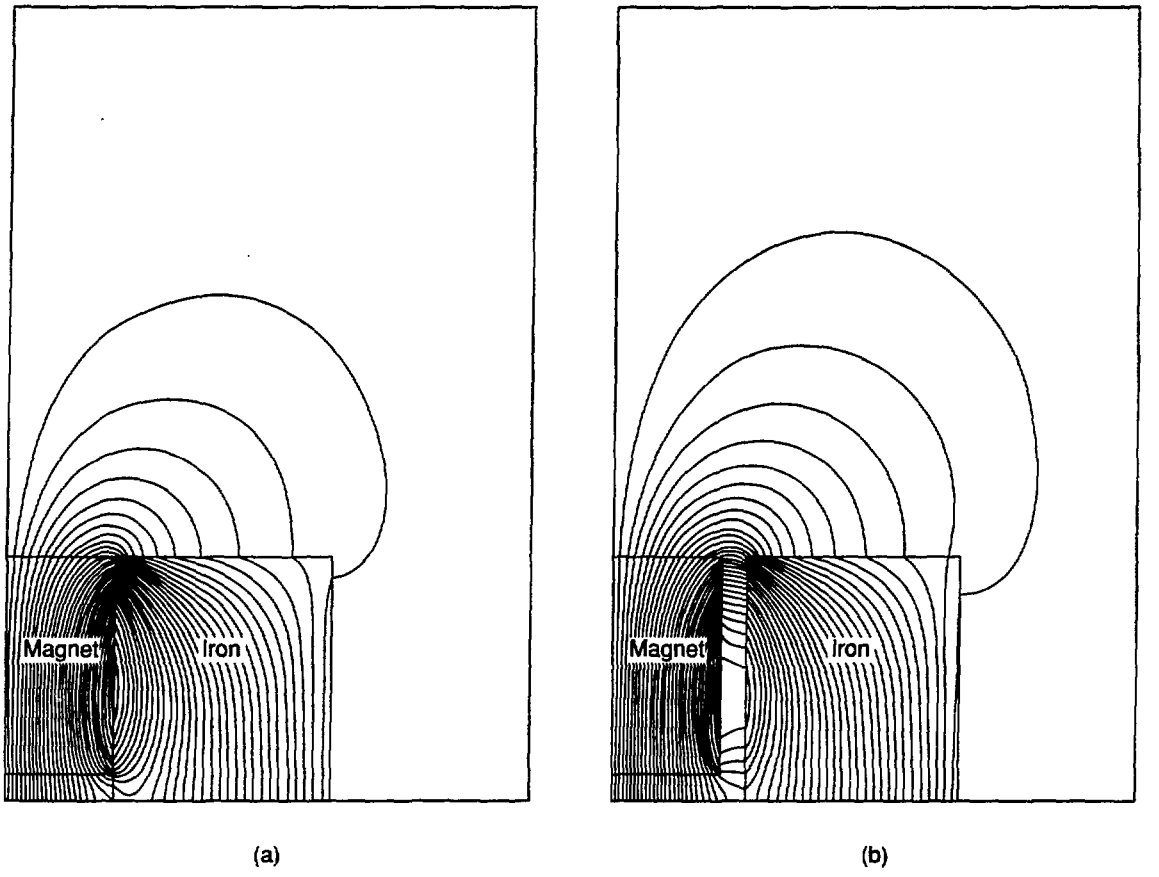

Figure 17: Poisson runs demonstrating the performance of a permanent magnet near iron (a) magnet touching iron (b) magnet not touching iron.

6. Conclusion

From the results presented, use of an elliptically polarized wiggler looks like a viable way to achieve 3–12 KeV circularly polarized X-rays from the NSLS X-ray ring. Other concepts, such as cross field undulator[4] or a bending magnet will either not yield the high photon energy required or will not produce enough photon flux. These approaches are more sensitive to the electron beam angular spread and hence they are not appropriate for the NSLS ring, which has low vertical β in its straight section. In order to increase the sensitivity of detection, AC modulation of the polarization is recommended. This can be done in an elliptical wiggler by constructing one of the wigglers from electromagnets and operating it with AC current. Two concepts for such a configuration were checked and

found to be feasible from the point of view of producing enough magnetic field.

There are several issues to be studied in a more detailed design:

1. A thorough three-dimensional design of the magnet configuration that will include study of eddy currents in the electromagnet core, the permanent magnets (and the effect on their magnetization) and the vacuum pipe walls.
2. A study of the orbit stability of an electron beam passing through an AC wiggler magnetic field in a storage ring. This study should include beam correction issues and control issues.
3. The polarized insertion device could also be operated as an undulator by opening the vertical wiggler gap. In this mode, the device will produce low energy circularly polarized X-rays. A study should be carried out to determine the performance of the device in the NSLS X-ray ring.

Although the X-ray ring has a low vertical β in its straight sections, the elliptical wiggler will yield sufficient circularly polarized light. Examination of the possibility of reducing the vertical emittance and/or increasing the vertical β is recommended because an improvement in the vertical angular spread would significantly improve the polarization output of the device.

Acknowledgement

We wish to thank M. Blume, D. Gibbs, K. Halbach, J. Hastings, K.J. Kim, D. McWhan and P. Siddons for helpful discussion.

7. References

1. N. Sakai, O. Terashime and H. Sekizawa, Nucl. Instrum. and Methods, Phys. Res. Sect. B **221**, 419 (1984).
2. F.W. Lipps and H.A. Tolhoek, Physica (Utrecht) **20**, 395 (1954).
3. A. Gover and A. Friedman, to be published.
4. K.J. Kim, AIP conference proceedings **185**, 565 (1987).
5. J.D. Jackson, "Classical Electrodynamics" 2nd edition, Wiley (1975).
6. S. Yamamoto, T. Shioga, S. Sasaki and H. Kitamora, Rev. Sci. Instrum. **60** (7), 1834 (1989).
7. S. Yamamoto, H. Kawata, H. Kitamora and M. Ando, PRL **62** (23), 2672 (1989).
8. K. Halbach, J. Chin, E. Hoyer, H. Winick, R. Cronin, J. Yang and Y. Zambre, Proc. of the 1981 Particle Accelerator Conf.
9. K. Halbach, NIM **A250**, 115 (1986).
10. E. Blum, "Development of an Undulator radiation Source for the Cornell Electron Storage Ring", UMI, Ann Arbor (1989).
11. C. Poloni, R. Brocco, B. Diviacco, R.P. Walker and D. Zangrando, Proc. of the 1991 PAC.
12. S. Krinsky, M.L. Perlman and R.E. Watson, "Characteristics of Synchrotron Radiation and of its Sources", Handbook on Synchrotron Radiation, Vol. 1A, Ed. E.E. Koch, North-Holand, New York (1983).
13. B.M. Kincaid, J. Appl. Phys. **48**, 2648 (1977).
14. D.F. Alferov, Yu.A. Bashmakov and E.G. Bessnov, Sov. Phys. Tech. Phys. **18**, 1336 (1974).
15. "Macsyma^{TM} User's Guide", Symbolics, Inc. (1988).
16. L.B. Felsen and N. Marcuvitz, "Radiation and Scattering of Waves", Prentice Hall, Engelwood Clifs, New Jersey (1973).
17. M. Born and E. Wolf, "Principles of Optics", 6th Edition, Pergamon Press, New York (1989).

18. M. Blume and Kistner, Phys. Rev. **171**, 14 (1968).